Materials & Design 220 (2022) 110837

Contents lists available at ScienceDirect

Materials & Design

journal homepage: www.elsevier.com/locate/matdes

TPU-based antiplatelet cardiovascular prostheses prepared using fused deposition modelling

Juan Domínguez-Robles [a], Emilia Utomo [a], Victoria A. Cornelius [b], Qonita Kurnia Anjani [a], Anna Korelidou [a], Zoilo Gonzalez [c], Ryan F. Donnelly [a], Andriana Margariti [b], Marc Delgado-Aguilar [d], Quim Tarrés [d], Eneko Larrañeta [a,*]

[a] School of Pharmacy, Queen's University Belfast, Lisburn Road 97, Belfast BT9 7BL, UK
[b] Wellcome-Wolfson Institute for Experimental Medicine, Queen's University Belfast, Belfast BT9 7BL, UK
[c] Chemical Engineering Department, BioPrEn Group (RNM 940), Instituto Universitario de Nanoquímica (IUNAN), Universidad de Córdoba, Córdoba 14014, Spain
[d] LEPAMAP Research Group, Department of Chemical Engineering, University of Girona, Spain

HIGHLIGHTS

- 3D-printing was used to prepare TPU vascular grafts loaded with dipyridamole.
- TPU samples containing 5% dipyridamole showed antiplatelet properties.
- TPU samples containing higher drug loadings did not show antiplatelet properties.
- The samples showed similar mechanical properties to previously described grafts.
- The resulting 3D-printed samples were hemocompatible.
- Samples loaded with 5% dipyridamole stimulated HUVEC cell proliferation.

GRAPHICAL ABSTRACT

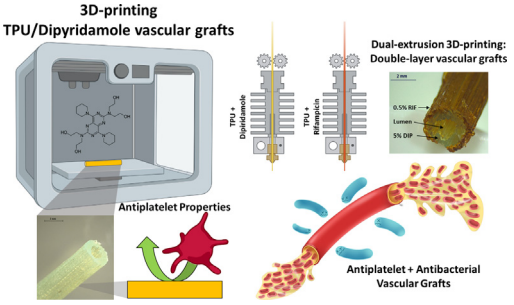

ARTICLE INFO

Article history:
Received 15 December 2021
Revised 6 June 2022
Accepted 7 June 2022
Available online 9 June 2022

Keywords:
Thermoplastic polyurethane
Fused deposition modelling
3D printing
Vascular grafts
Dipyridamole
Antiplatelet materials

ABSTRACT

This work describes the use of fused deposition modelling (FDM) to prepare antiplatelet thermoplastic polyurethane (TPU)-based tubular grafts. FDM 3D-printing technology is widely available and provides the ability to easily design tubular grafts on demand, enabling the customisation of vascular prosthesis dimensions. An antiplatelet drug, dipyridamole (DIP), was combined with TPU using hot-melt extrusion to prepare filaments. DIP cargos ranged between 5 and 20% (w/w). The resulting filaments were used to prepare small diameter vascular grafts using FDM. These grafts were characterised. Moreover, DIP release kinetics, antiplatelet activity and in vitro hemo- and cytocompatibility were evaluated. The results suggested that the materials could provide sustained DIP release for 30 days. Moreover, the presence of 5% DIP in the material showed a clear antiplatelet effect compared with pristine TPU. Alternatively, higher DIP loadings resulted higher surface roughness leading to higher platelet adhesion. Therefore, the biocompatibility of 5% DIP samples was tested showing that this type of materials allowed higher HUVEC cell proliferation compared to pristine TPU samples. Finally, DIP loaded TPU was combined with rifampicin-loaded TPU to prepare double-layered tubular grafts. These grafts demonstrated a clear antimicrobial activity against both *Staphylococcus aureus* and *Escherichia coli*.

* Corresponding author.
E-mail address: e.larraneta@qub.ac.uk (E. Larrañeta).

https://doi.org/10.1016/j.matdes.2022.110837
0264-1275/

1. Introduction

Cardiovascular disease refers to a number of vascular conditions that combined are the leading cause of death globally [1,2]. The prevalence of this set of conditions is expected rise and result in the mortality of 23.6 million people by the year 2030 [3]. Cardiovascular tissue in adults is not capable of self repairment or regeneration following injury, as such in the later stages of cardiovascular disease the only therapeutic option is transplantation or replacement of organs or tissues [4]. To fight cardiovascular disease while improving patient's life expectancy and quality of life different types of cardiac implants have been developed [5]. These type of devices include stents, valvular prostheses, cardiac patches and vascular grafts among others [6,7].

Vascular grafts are implantable devices that are used to bypass a defective blood vessel [8]. The first line of treatment for bypass surgery is to use autologous vessels [9–11]. However, harvesting autologous vessels is invasive and in some cases unsuitable [12]. As such, synthetic polymeric vascular grafts have been developed [13,14]. Whilst they have successfully been used to replace large blood vessels [15,16], they have demonstrated limited success when used to replace small diameter vessels (lower than 6 mm internal diameter) [3,15,17]. The main associated complication is the blocking of the grafts due to thrombosis and intimal hyperplasia [18]. In order to prevent these complications, drug loaded vascular grafts have been used [19]. Drugs such as heparin, cilostazol, dipyridamole (DIP) or acetylsalicylic acid have previously been loaded into vascular grafts to prevent the formation of blood clots [20–24]. In order to prepare medicated vascular grafts several types of techniques have emerged including electrospinning, mould-casting and 3D printing [3,25]. An advantage of 3D printing over the other techniques, however, is its ability to create devices with different shapes and sizes in a simple and rapid way [26].

3D printing or additive manufacturing (AM), is a family of techniques that are used to prepare 3D objects by adding successive layers of material in a sequential way [26,27]. This type of technology has been extensively used in medicine to create patient-specific models and prostheses [28]. One of these techniques that has been heavily used due to its low cost and availability is fused deposition modelling (FDM) [29]. FDM uses thermoplastic filaments that are extruded from a heated nozzle [29]. The material melts in the nozzle and is deposited in layers to form a 3D object [29]. The simplicity of this technology has made it globally available [30]. Consequently, the development of medical applications using this type of AM technology could have a great potential impact in developing countries due to its simplicity and affordability [31].

Drugs or other active molecules can be added to the thermoplastic using hot-melt extrusion to prepare drug loaded filaments [32]. Accordingly, FDM has been used to prepare a wide variety of pharmaceutical products and medical devices [33–38]. There is a wide variety of thermoplastic polymers that can be used for FDM applications including biocompatible polymers such as poly (lactic acid), poly(propylene), poly(ether ether ketone) or thermoplastic polyurethane (TPU) among many others [39]. In particular, TPU is a beneficial material for biomedical applications due to its elastomeric properties [40]. As such, TPU has previously been used for medical implants including the development of vascular grafts [41–43].

This work describes the use of FDM for the development of small-diameter TPU-based vascular grafts with antiplatelet properties. For this purpose, TPU was extruded with different concentrations of DIP to obtain filaments for FDM applications. The resulting filaments were characterised and used for FDM production of vascular grafts. The resulting 3D-printed objects were characterised using different techniques to evaluate their physicochemical properties, hemocompatibility, antiplatelet activity and cytocompatibility. In a previous work we described the use of FDM for the preparation of TPU-based vascular grafts [34]. However, this was a proof of concept study as drug loadings were low (<2%). The present study presents an improve technique to produce TPU-based materials for FDM applications. Moreover, in this work we provide evidences of the antiplatelet activity of the resulting materials. The results of this study highlight the importance of the use of affordable technology that can be used in the development of future therapies.

2. Materials and methods

2.1. Materials

Elastollan® thermoplastic polyurethane (TPU) from BASF (shore hardness of 80A) was donated by DistruPol Ltd (Dublin, Ireland). Dipyridamole (DIP) and rifampicin (RIF) were purchased from Tokyo chemical Industry (Oxford, UK) and Alfa Aesar (Lancashire, UK), respectively. Castor oil was obtained from Ransom (Hitchin, UK). Rabbit blood in sodium citrate was provided from Rockland (Reading, UK). Ethanol was obtained by Sigma-Aldrich (Dorset, UK). Glutaraldehyde 25% EM Grade was provided from Agar Scientific Ltd. (Essex, UK). Phosphate buffer solution (PBS) was obtained from VWR Chemicals (Ohio, USA). All materials and reagents were used as received. *Escherichia coli* NCTC 10,418 and *Staphylococcus aureus* NCTC 10,788 were both used and incubated over-night at 37 °C in Mueller–Hinton (MH) broth for performing the disk diffusion test.

2.2. TPU composite preparation

The incorporation of DIP within the TPU matrix was carried out before the extrusion of the DIP-loaded filaments in order to obtain a homogeneous distribution throughout the entire material. This

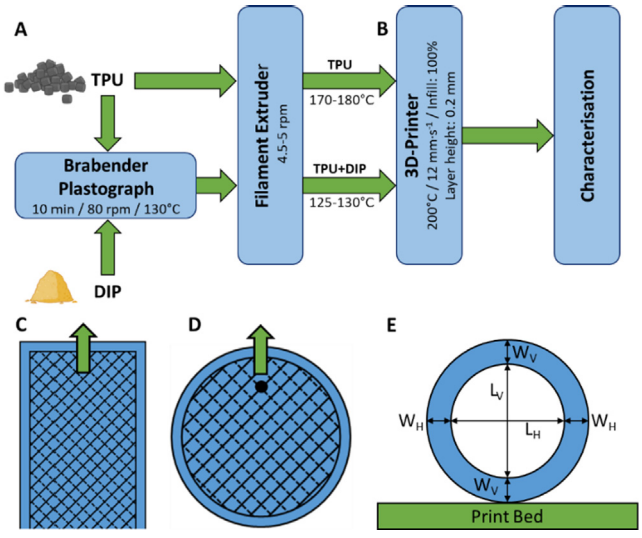

Fig. 1. Diagram containing the different experimental phases, including mixing, hot-melt extrusion (A) and 3D-printing (B), used to prepare the 3D-printed small-diameter vascular grafts. Designs of the 3D printing strips (C) and discs (D) used to evaluate the uniaxial tensile mechanical properties and the suture retention strength test of the 3D-printed materials, respectively. The arrow indicates the tension direction during mechanical testing. Diagram showing the cross-section of a vascular graft and the different dimensions that were evaluated and presented in Table 1(E).

process is summarised in Fig. 1A. The pre-extrusion of the material using a plastograph Brabender (Brabender GmbH & Co KG, Brabender Plastograph EC, Germany) allowed the incorporation of high DIP contents (up to 20%), while maintaining the homogeneity of the resulting material. For this purpose, TPU was completely dried for a minimum of 48 h at 80 °C in an oven before processing. Initially, the mixing chamber of the plastograph Brabender was preheated to 130 °C. The required amount of TPU was then added while maintaining the rotation of the twin-screw constant at 80 rpm. Once the TPU reached the melting point, determined by decreasing the torque, the required DIP amount was added and the agitation and temperature maintained for 10 min. At the end of the mixing time, the plastograph compartment was opened and the mixture discharged. Finally, once the material was completely cooled, it was milled using a blade mill (IKA, MF 10.2 Impact grinding, France) into particles of approximately 5 mm and kept in the tank at 80 °C until further processing.

2.3. TPU filament production

TPU-based filaments for 3D printing were prepared using a filament extruder 3devo model NEXT 1.0 (3devo, Utrecht, The Netherlands). The extruder is capable of extruding a filament with a diameter of 2.85 mm diameter, which can be then used for 3D printing. The extruder is equipped with four heating areas, which were set between 170 °C and 180 °C for TPU, and between 125 °C and 130 °C for those DIP-loaded filaments (Fig. 1A). Moreover, the extruder speed was set at 4.5–5 rpm regardless of the material composition. The TPU filament containing 0.5% RIF was manufactured using a previously described method by Weisman et al. [44]. In brief, however, TPU pellets were coated with RIF using castor oil as a coating oil, the drug coated pellets were then placed in a filament single screw extruder (3devo, Utrecht, The Netherlands), which was used to extrude the 0.5% Containing TPU filament. The extrusion temperatures were maintained between 170℃ and 200℃ through the four heaters located in the extruder. The extrusion speed was kept between 3 and 5 rpm. The filament diameter was 2.85 mm. The homogeneity of the final filaments was evaluated using a Leica EZ4 D digital microscope (Leica, Wetzlar, Germany).

2.4. 3D-printed objects design and manufacture

Multiple objects, including discs, rectangular-shaped strips and tubular grafts were designed using a computer-aided design (CAD) software and printed using the Ultimaker 3 (Ultimaker B.V., Geldermalsen, Netherlands) equipped with a 0.4 mm nozzle. Moreover, Cura® 3.0 software was used for this 3D printing process. The print temperature was 200 ℃, the print speed used was 12 mm/s, the layer height was 0.2 mm and the infill density was set at 100% for the different TPU filaments containing DIP. The printing parameters for TPU and TPU combined with DIP can be seen in Fig. 1B. Vascular grafts were printed longitudinally as described previously [21]. In addition to vascular grafts other objects such as discs or mechanical testing specimens were printed. The slicing parameters for the Cura® 3.0 software were the same for all the objects. However, due to the larger size the infill pattern obtained for larger objects was the one included in Fig. 1C and D. Alternatively, a TPU filament containing 0.5% RIF was used in the second extruder to prepare a double-layered tubular graft from the same 3D printer. The inner layer was made from the TPU filament containing 5% DIP and the outer layer was made from the above-mentioned TPU filament containing 0.5% RIF. For the latter, the printing temperatures were between 215 ℃ and 220 ℃, the layer height was set at 0.1 mm and the printing speed remained the same, as previously published by Martin et al. [34]. The wall thickness and lumen diameter of the DIP containing tubular grafts were evaluated using a Leica EZ4 D digital microscope (Leica, Wetzlar, Germany) as described in Fig. 1E. The digital microscope was also equipped with NIGHTSEA Model SFA Stereomicroscope Fluorescence Adapter with the Royal Blue excitation/emission to obtain fluorescence images of the double-layer tubular graft.

2.5. Characterisation of 3D-printed materials

2.5.1. Microscopy

Surface morphology of the 3D-printed materials was evaluated by using scanning electronic microscopy (SEM) (Hitachi TM3030; Tokyo, Japan). The topography of 3D-printed surfaces, also known as surface texture or surface finish was also analysed by using a 3D surface metrology microscope DCM8 (Leica Microsystem, Weztlar, Germany).

2.5.2. Contact angle goniometry (CAG)

The influence of the DIP on the contact angle of deionised water with the surface of the 3D-printed materials was evaluated using an Attension Theta equipment (Attension Theta, Biolin Scientific, Gothenburg, Sweden). Moreover, OneAttension software was used to analyse the results [45,46]. Each reported contact angle is a mean of four measurements. The volume of each droplet used was kept constant (≈4 μL) and each contact angle reported was measured 30.24 s after release of the droplet.

2.5.3. Fourier transform infrared (FTIR) spectroscopy

Fourier transform infrared (FTIR) spectra of the 3D-printed materials and the pure DIP were recorded using a Spectrum Two instrument (Perkin Elmer, Waltham, MA) to evaluate if any interactions had occurred between TPU and DIP. For this purpose, attenuated total reflectance (ATR) technique was used and the resulting spectra recorded from 4000 to 600 cm^{-1} with a resolution of 4 cm^{-1}. A total of 32 scans were collected.

2.5.4. X-ray diffraction (XRD) analysis

The crystalline structure of the 3D-printed materials was evaluated by XRD analysis. This test was carried out using MiniFlex II Dekstop Powder X-ray diffractometer (Rigaku Corporation, Kent, UK) equipped with Cu Kβ radiation. The scanning was performed for 2.0°/min with an angular range of 5–60° 2θ (2 theta) in continuous mode with a sampling width of 0.03°at room temperature. The current used was 15 mA and the voltage 30 kV.

2.5.5. Thermal analysis

Thermal properties of the 3D-printed materials and the pure DIP were evaluated by performing thermogravimetric (TGA) and differential scanning calorimetry (DSC) analysis. A Q50 thermogravimetric analysis instrument (TA instruments, Bellingham, WA, USA) was used for TGA to establish the degradation temperatures of the 3D-printed materials and the pure drug to ensure no degradation would take place when exposed to the high temperatures during the extrusion or printing process. Small pieces of the 3D-printed materials (between 3 and 10 mg) were heated at a rate of 10 ℃/minute from room temperature to 450 ℃ under a nitrogen flow rate of 40 mL/min. Moreover, a Q20 differential scanning calorimeter (TA instruments, Bellingham, WA, USA) was used to evaluate drug-polymer interactions and establish if DIP was forming an amorphous dispersion after mixing with the TPU matrix. For this purpose, the drug powder and small pieces of the 3D-printed materials were analysed from 30 ℃ to 300℃ at a heating rate of 10 °C/min, under a nitrogen flow rate of 40 mL/min.

2.5.6. Mechanical testing

The uniaxial tensile mechanical properties of the filaments and the 3D-printed materials were tested and compared using a TA. XTplus texture analyser (Stable Micro Systems, Surrey, UK) at a constant extension speed of 10.2 mm/min [21]. For this purpose, the strips were printed as shown in Fig. 1C. The diameter of the filaments and the thickness of the strips were measured using a calliper to calculate the cross-sectional area, and both the filaments and the strips were clamped with an inter-clamp distance of 20 mm. Force displacement curves were recorded and different parameters were calculated from these curves. The offset yield strength of both the filaments and the 3D-printed strips was obtained using the 0.2% offset method, as an approximation of the material's elastic limit [36,47]. Additionally, the elastic modulus was obtained as the slope of the initial linear region of the stress/strain curve [48,49]. Moreover, the ultimate tensile strength (UTS) and elongation at failure was obtained by generating the stress/strain curves of the tested strips [49].

For the suture retention strength test, 3D-printed discs of 13 mm diameter were printed as shown in Fig. 1D. The thickness of each disc was measured using a calliper to calculate its cross-sectional area. The bottom end was fixed, and a 4/0 Ethilon Polyamide 6 suture thread (Ethicon Inc., Somerville, NJ) was passed through a hole located 3 mm apart from the edge of the 3D-printed disc. The suture thread was extended on a TA.XTplus texture analyser under the same conditions as the above tensile test (a controlled speed of 10.2 mm/min), until the disc was entirely ripped. The suture retention strength was calculated as load force (N)/(suture diameter (mm) × sample thickness (mm)) [23].

2.6. Drug release study

The release study of DIP loaded tubular grafts was conducted by introducing a weighed piece of a tubular graft (1 cm in length) into a glass vial containing different volumes of the release medium (PBS) for each concentration, in order to maintain sink conditions. The vials were placed into an incubator at 37 °C and shaken at 40 rpm as reported previously [50,51]. Samples of the release medium were taken at specified time points (24–48 h) and the concentration of DIP was analysed using fluorescence spectroscopy (FLUOstar Omega Microplate Reader, BMG LABTECH, Ortenberg, Germany). The excitation and emission wavelengths used were 280 nm and 460 nm [23]. After each measurement, samples were dried and placed in fresh PBS. All the reported time points are a mean of four measurements over 30 days.

2.7. Platelet adhesion study

Blood platelet deposition on the 3D-printed sample surface was measured using rabbit platelet-rich plasma (PRP), which was produced by centrifuging the rabbit blood in sodium citrate (Rockland Immunochemicals, Inc; Pottstown, PA, USA) at 1840 rpm for 15 min [52]. Discs of 5 mm diameter and 1 – 2 mm of thickness containing either no drug or 5%, 10% or 20% of DIP, and placed in a 96-well plate. Subsequently, samples were incubated with a 200 μL aliquot of the PRP at 37 °C for 2 and 6 h. After each incubation time, samples were rinsed three times with PBS and fixed with a 2.5% glutaraldehyde solution for 2 h. After washing three times with PBS, samples were dehydrated through a series of ethanol solutions (70% and 100%) for 15 min at each step. After this dehydration step, the samples were allowed to dry at room temperature for 24 h. Finally, SEM (Hitachi TM3030; Tokyo, Japan) micrographs ($n \geq 3$) were used to count the adhered blood platelets on the scaffold surface.

2.8. Hemocompatibility study

A hemolysis test was made using rabbit blood in sodium citrate (Rockland Immunochemicals, Inc; Pottstown, USA) to assess the effect of the 3D-printed materials on red blood cells (RBCs) [34,53]. In brief, 1 mL of blood was poured into a 1.5 mL Eppendorf tube, which was centrifuged at 2000*g* for 5 min. The supernatant was discarded, and the resulting pellet resuspended in 1 mL of a saline solution (0.9% NaCl solution). This procedure was repeated 3 times. The resuspended pellet, in 1 mL of saline solution or distilled water (for the positive control), was then transferred to a vial containing 9 mL of saline solution or water, respectively. After this step, a small 3D-printed disc of 5 mm diameter and 1 – 2 mm of thickness was placed in a 1.5 mL Eppendorf tube for the hemolytic evaluation. Subsequently, 200 μL of the previous diluted blood solution was added to the tube containing the 3D-printed construct. The tubes were incubated for 1 h at 37 °C and then centrifuged at 2000 *g* for 5 min. Afterward, the supernatant was carefully collected and transferred into a 96-well plate to measure the absorbance at 545 nm using a UV/vis spectrometer (FLUOstar Omega Microplate Reader, BMG LABTECH, Ortenberg, Germany) [23,54]. Moreover, the absorbance 545 nm of the diluted blood in both 0.9% NaCl solution (negative control) and distilled water (positive control) was also measured. The percentage of hemolysis or hemolysis ratio was calculated by Equation (1).

$$\%\ Hemolysis\ =\ 100\ \times\ (A_S - A_N)/(A_P - A_N) \quad (1)$$

where A_S is the absorbance value of the test sample, and A_N and A_P are the absorbance values of negative and positive controls, respectively.

2.9. Huvecs growth

To assess cellular compatibility, following sterilisation and calibration as we previously described [21,34], 20,000 human umbilical vein endothelial cells (HUVECs) (ATCC CRL-1730), resuspended in 80 μL of media, were seeded in a dome on top of each scaffold, allowing for direct settlement of cells onto the graft, and incubated at 37 °C with 5% CO_2. After an 8-hour attachment period the scaffolds were submerged in cell culture media (EGM-2 media (LONZA 00190860)). Cells were subsequently cultured for an additional 48 h to evaluate biocompatibility. Cellular attachment was assessed through light microscopy. In addition, cellular viability and proliferation were detected through staining with Vybrant™ DiI cell labelling solution (Thermo Fisher Scientific V22885) and the performance of a CyQUANT™ NF Cell Proliferation Assay (Thermo Fisher Scientific, C35006). Furthermore, to evaluate the effect on cellular morphology, immunofluorescence staining for CD144 (ab33168), an endothelial cell barrier marker, was performed on HUVECs fixed to the scaffold.

2.10. Microbiological assay

A double-layer tubular graft was tested for inhibitory effects on bacterial cultures of *Staphylococcus aureus* NCTC 10,788 (Gram-positive) and *Escherichia coli* NCTC 10,418 (Gram-negative). The inner layer of the graft consisted of the TPU filament containing 5% DIP and the outer layer was made from the TPU filament containing 0.5% RIF. Moreover, a tubular graft containing 5% DIP was used as a negative control. For this purpose, the above-mentioned tubular grafts were cut into slices of 2 mm (n = 4). These slices were then placed in a UV transilluminator (UVP, California, USA) in 'high' mode and each side was illuminated for 15 min. Inoculated plates for each bacterial strain were also incubated as a positive control. This in vitro microbiological assay was performed according to previous published work, with some mod-

ifications [34,55]. In brief, both bacterial strains were incubated in Mueller–Hinton (MH) broth overnight. After which, 50 μL of the culture was added to 5 mL of soft MH agar, the mixture vortexed and then poured on top of the MH agar plate. Slices of the tubular grafts were then placed on top of the agar and incubated at 37 ℃ for 24 h. The zone of inhibition caused for both bacterial strains was measured in mm. The results were expressed as mean ± standard deviation of 4 replicates.

2.11. Statistical analysis

All quantitative data are expressed as a mean ± standard deviation. Statistical analysis was performed using a one-way analysis of variance with Tukey's post-hoc. For the platelet adhesion study, when the samples were incubated with a 200 μL aliquot of the PRP for 6 h, a samples *t*-test was used. Finally, a *t*-test was used to compare cell proliferation for TPU and 5% DIP samples.

3. Results and discussion

3.1. Preparation and characterisation of DIP-loaded TPU filaments

A pre-extrusion step was performed for the addition of high DIP contents (up to 20%) while maintaining the homogeneity of the resulting materials by using a plastograph Brabender. Following, HME was used to prepare DIP-loaded filaments for FDM applications. The filaments were evaluated using a light microscope (Leica, Wetzlar, Germany) and the yellow colour found to proportionally darken as the amount of DIP increased, thus confirming an increased amount of DIP is present in the performed filaments (Fig. 2A). Moreover, it can be interfered that the drug was successfully mixed with the TPU matrix. The filaments were homogeneous, showing no visible DIP aggregates. Only small irregularities were observed for the filaments containing 10% and 20% DIP. Thus, indicating that a complete mixing process had taken place within both the pre-extrusion and single screw extruder due to the high temperature and high shear forces created by the rotating screw actions [56]. Additionally, the resulting filaments had a diameter ranging between 2.70 and 2.85 mm (Fig. 2A).

Elastic modulus and the offset yield strength of the TPU and DIP containing filaments were measured (Fig. 2B-C). The incorporation of DIP into the material had a direct influence on the mechanical properties of the filament only when the drug content is at least 20% (w/w). The elastic modulus of filaments containing 20% (w/w) of DIP was higher than the elastic modulus of the filaments containing no drug and 5% (w/w) of DIP ($p < 0.05$). Additionally, it can be concluded that filaments containing no drug, 5% and 10% of DIP (w/w) showed equivalent elastic modulus values ($p > 0.05$). The same behavior can be observed for the offset yield strength (Fig. 2C). The elastic modulus values obtained for the filaments containing no drug, 5% and 10% are in line with other published works that used the same type of TPU [34]. The influence of higher drug loading on the mechanical properties of the material has been reported before for other drugs such as theophylline [57]. Additionally, it has been reported before that lower drug content does not affect the mechanical properties of the resulting material [34,55].

3.2. Preparation and physicochemical characterisation of 3D-printed samples

These filaments were used to prepare different 3D-printed materials, including tubular grafts, by FDM. As mentioned above, 3D-printed materials were completely homogeneous and DIP dissolved into the TPU matrix. DIP has reported antiplatelet properties [21,23,34,58] and thus can be used to prevent the formation of blood clots on the inner surface of these tubular grafts. Accordingly, small-diameter vascular grafts (<6 mm diameter) containing different DIP concentrations were manufactured using FDM. The design of the small-diameter vascular grafts included a lumen diameter of 2 mm and a wall thickness of 0.5 mm. Table 1 shows the dimensions of these tubular grafts. Moreover, Fig. 3 shows representative light microscope pictures of the resulting 3D-printed small-diameter vascular grafts. The results displayed in the Table 1 shows that in all the cases, the 3D-printed tubular grafts showed some deviation from the CAD original model. These deviations are clearly related to the higher amount of DIP present in the tubular grafts. Both dimensions, vertical lumen (L_V) and horizontal lumen (L_H) (Fig. 1E) decrease as the amount of DIP increases. On the contrary, the wall thickness, in all the measured points, increases as the amount of DIP decreases. Moreover, no significant differences were found in the grafts dimension printed using only TPU or containing 5% DIP (w/w) ($p > 0.05$). Only the horizontal wall thickness (W_H) graft dimension values for these two samples presented significant differences ($p < 0.05$). Additionally, these samples had closer values to the CAD original model than the ones containing 10% and 20% DIP (w/w). However, this deviation could be corrected with printing by adjusting the distance between the nozzle and the build surface of the 3D printer (Z offset) before starting the process [21]. Additionally, another strategy to achieve

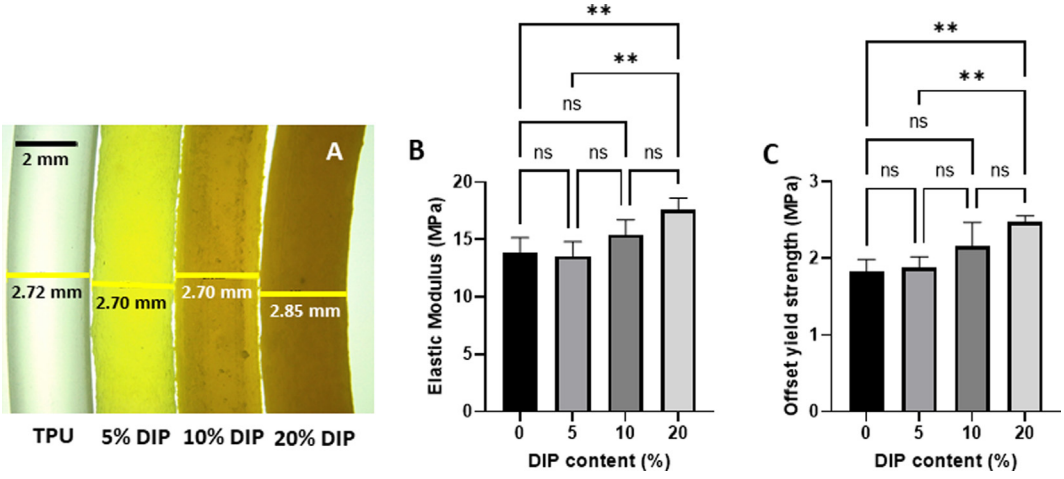

Fig. 2. Light microscope image of the DIP-loaded TPU-based filaments (A). Elastic modulus (B) and offset yield strength (C) of the extruded filaments (n = 4).

Table 1
Dimension of the 3D-printed tubular grafts (n ≥ 4). L_H, L_V, W_V and W_H definition can be found in Fig. 1E.

	3D printed model distance (mm)			
	L_V	L_H	W_V	W_H
CAD Model	2	2	0.5	0.5
TPU	2.13 ± 0.13	1.69 ± 0.08	0.50 ± 0.08	0.59 ± 0.05
5% DIP	1.90 ± 0.07	1.67 ± 0.14	0.52 ± 0.10	0.77 ± 0.06
10% DIP	1.45 ± 0.11	1.55 ± 0.07	0.65 ± 0.20	0.92 ± 0.13
20% DIP	0.95 ± 0.15	1.20 ± 0.10	0.88 ± 0.29	1.23 ± 0.08

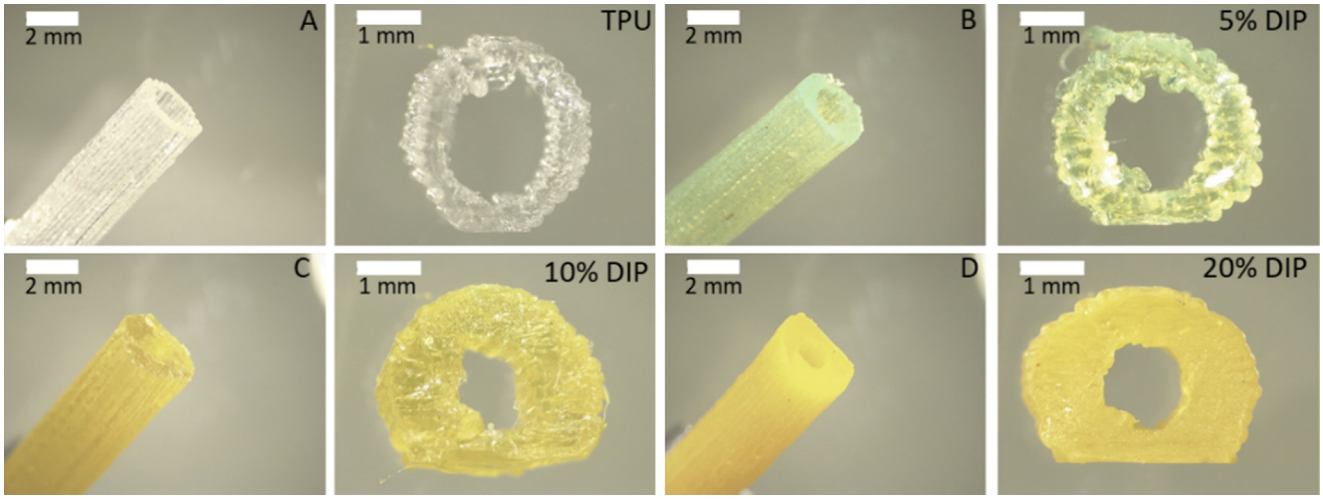

Fig. 3. Light microscope images of the 3D-printed tubular grafts and their cross-sections. Scale bars are 1 and 2 mm.

the required dimension of the 3D-printed object is to take account of these deviation when designing the CAD file [34]. Despite these deviations, FDM has been successfully used for precision procedures including the development of surgical guides [59]. Additionally, other types of extrusion-based 3D printing technologies such as robocasting can be used to print similar systems (Fig. S1, supporting information). The main advantage of this type of 3D-printing is that it does not require an extrusion process to prepare a polymer/drug filament [21,22,60,61]. However, compared to FDM, this type of technology does not provide the same degree of control over layer deposition (Fig. S1, supporting information). Moreover, it is both more expensive and complex to use.

SEM was used to characterize the surface of the 3D-printed tubular grafts. SEM images (Fig. 4) showed that 3D-printed tubular grafts containing no DIP and 5% DIP had a smooth surface as no drug aggregates were observed. On the contrary, grafts containing higher DIP cargos (10% and 20%) showed higher surface roughness. Surface morphology can be affected by the drug concentration, as had been previously reported in the literature [23,62]. 3D-printed samples containing higher DIP concentrations (10% and 20%) showed higher opacity than samples made from TPU only or 5% DIP (Fig. 4). However, the cross-section of all the 3D-printed materials were homogeneous indicating a good integration of the drug and the polymer.

Considering that textural features of the of 3D-printed samples plays a crucial role in determining their mechanical and antiplatelet properties, the topographies of the prepared materials were additionally analysed in terms of waviness and lay of the exposed surfaces. Confocal microscopy images and topographic profiles of 3D-printed tubular grafts surfaces containing different DIP concentrations are presented in Fig. 5. Notice that waviness of tubular grafts is understood like a measure of surface irregularities with a spacing greater than that of the predominant pattern measured for roughness. On the other hand, it is important to remark that the lay of the exposed surfaces was analysed by the direction of the predominant surface pattern which has been fixed through the printing method. These results confirm the previous hypothesis described from SEM micrographs. While the 3D-printed structures containing no DIP and 5% DIP presented higher level of waviness with smoother surfaces, the samples containing 10% and 20% DIP showed higher roughness textures over the surface of the waves. The topographic profiles, studied on the highest points of the tubular grafts, evidences significant details related with their surface finish.

Contact angle measurements were used to gain additional information about the surface properties of the TPU-based 3D-printed samples. This measurement relates to the extent of hydrophobicity and hydrophilicity and may help to explain any differences in platelet adhesion [63–67]. Water contact angle with the surface of the 3D-printed samples is shown in Fig. 6A. The addition of higher DIP concentrations (10% and 20%) significantly increased surface hydrophilicity of the samples ($p < 0.05$). On the other hand, no significant differences were found for the contact angle values obtained for pristine TPU and samples containing 5% DIP (w/w) ($p = 0.639$). A similar behaviour has previously been reported for poly(urethane) biomaterials sprayed with DIP solution [68]. This decrease in the contact angle could be explained by the changes found in the surface morphology of the 3D-printed samples. As previously mentioned, the addition of DIP increased the roughness of the sample. This roughness may contribute to a higher surface wettability [45,69].

FTIR analysis was performed to evaluate any potential interactions between DIP and TPU within the samples (Fig. 6B). Pristine TPU samples showed characteristic peaks for the urethane group [34]. The peaks around 3300 and 1520 cm^{-1} are characteristic of the N-H group. On the other hand, a clear carbonyl peak can be

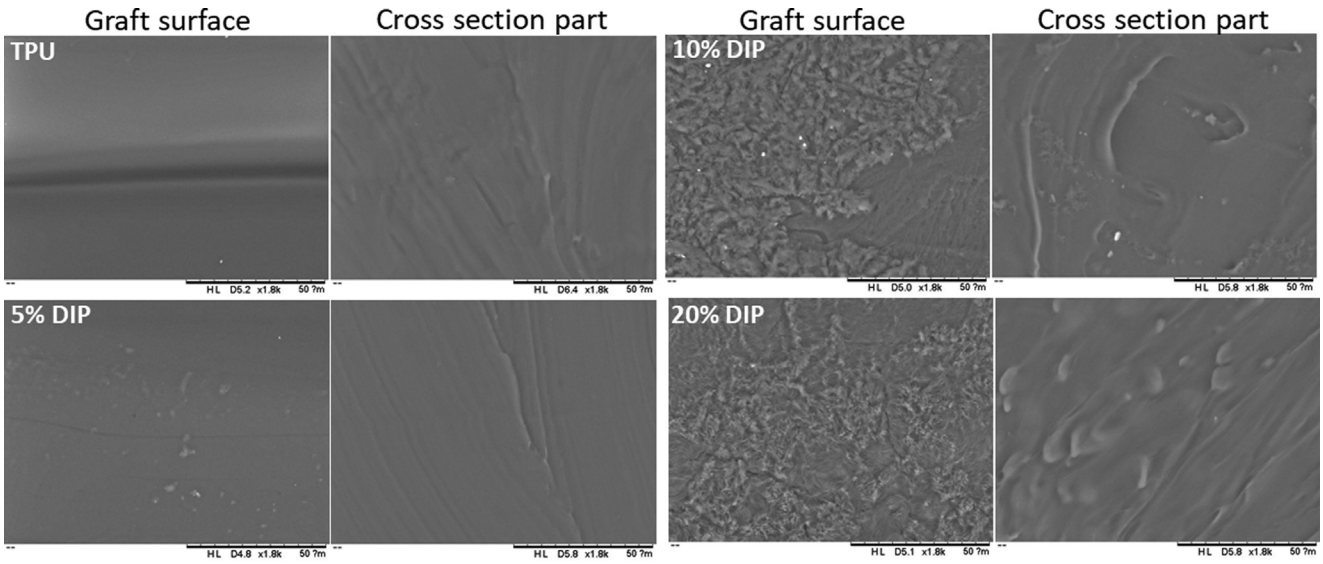

Fig. 4. SEM images of the 3D-printed tubular grafts surfaces containing different DIP concentrations and their cross sections.

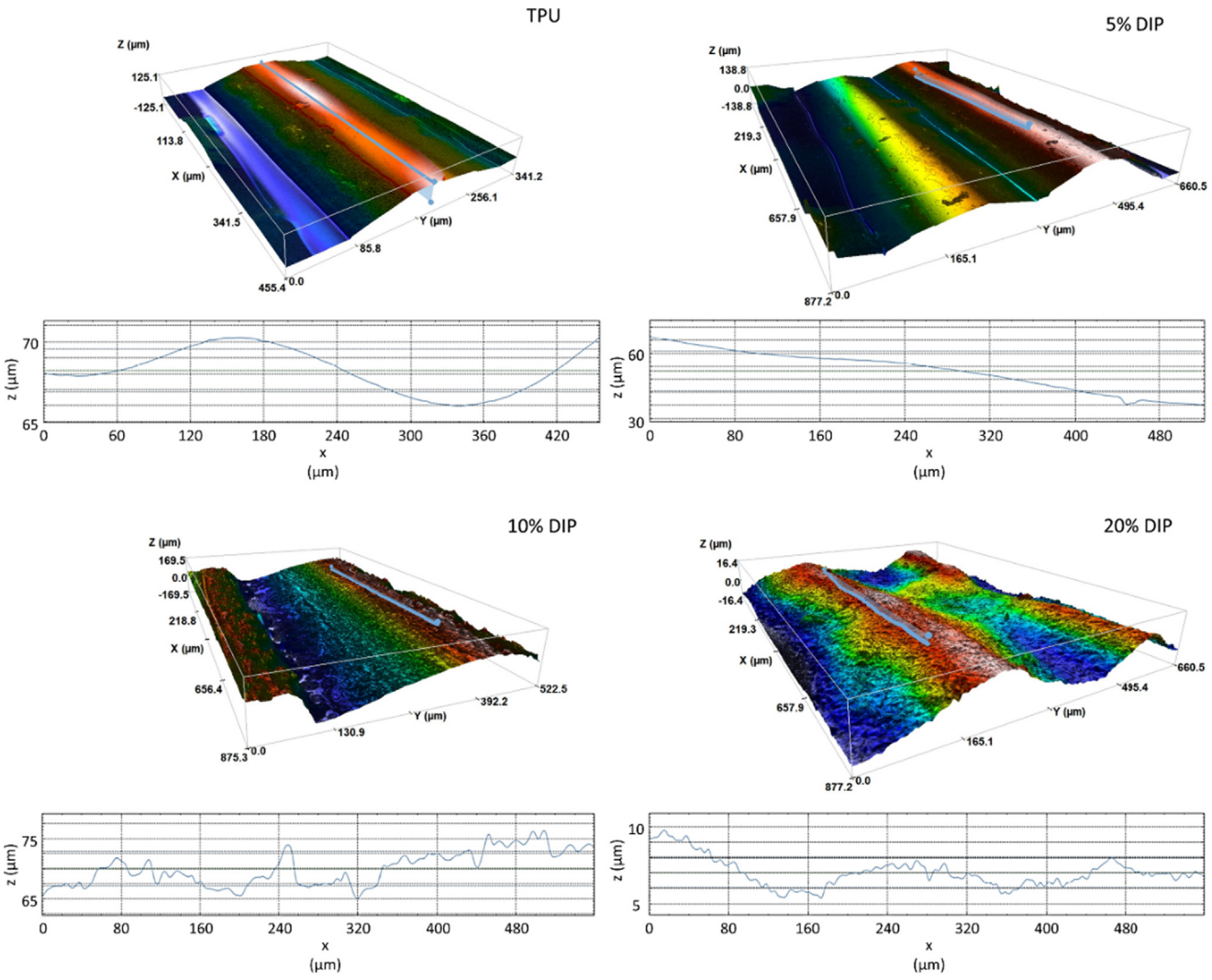

Fig. 5. 3D images of the tubular grafts' surfaces containing different DIP concentrations and their topographic profiles studied in the direction of the predominant surface pattern determined by the 3D printing methodology.

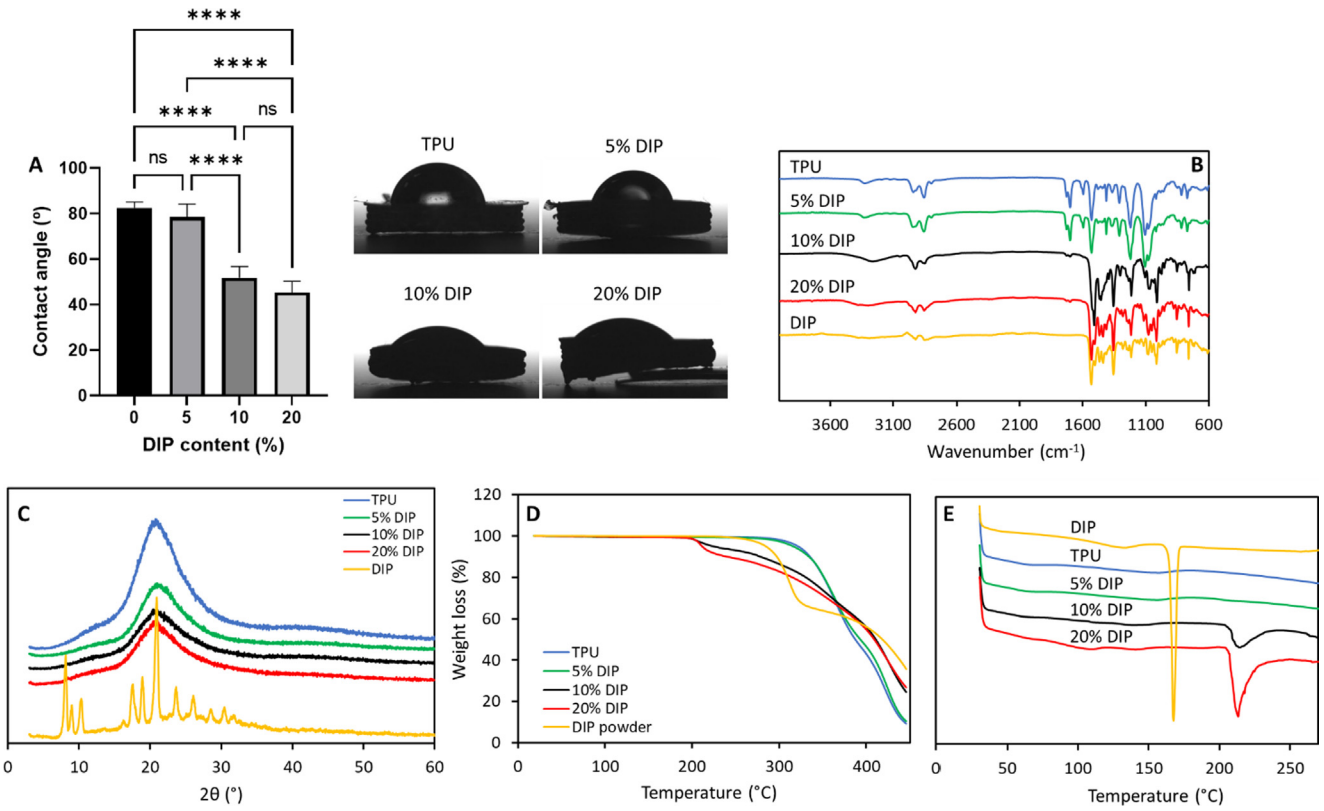

Fig. 6. Influence of the DIP content on the contact angle of water with the DIP-loaded 3D-printed samples (n = 4). ATR-FTIR spectra (B), XRD diffractograms (C) and TGA (D) and DSC curves (E) of each of the DIP-loaded 3D-printed samples.

seen around 1730 cm^{-1}. Additionally, CH stretching peaks at around 2900 cm^{-1} can be seen in the spectra of pristine TPU. Whilst, the DIP spectra showed a broad peak at around 3300 cm^{-1} that can be assigned to multiple –OH groups present in the molecule [70]. Moreover, DIP FTIR spectrum showed a characteristic peak at around 1530 cm^{-1} that can be attributed to the C-N bond within the heteroaromatic ring of this molecule [70]. DIP peaks can be found in the IR spectrum of 3D-printed samples containing DIP. No new peaks were obtained, suggesting that no chemical reactions took place, during the extrusion or 3D-printing processes. Interestingly, however, there were subtle changes in the bands around 3300 cm^{-1} and in the bands between 1500 and 1600 cm^{-1}. These changes suggest that non-covalent interactions are taking place between TPU and DIP. The changes observed in those bands suggest hydrogen bonds and interactions between the DIP heteroaromatic ring [70] and the aromatic rings within TPU chains [71].

XRD was used to evaluate the crystallinity of the 3D-printed samples. XRD diffractograms of pure DIP, TPU and DIP-loaded TPU 3D-printed samples are presented in Fig. 6C. Crystallinity of the formed 3D-printed samples was evaluated by comparing the representative peak of these samples with the pure DIP, as a reference. The diffractogram of DIP displayed several sharp peaks at the following diffraction angles (2θ) of 8.14°, 10.14°, 10.40°, 17.58°, 18.92°, 20.94°, 23.68° and 26.2°, which indicated that DIP is presented in a crystalline form. However, there were no diffraction peaks in the XRD diffractograms of the TPU 3D-printed samples, indicating that the polymeric matrix has an amorphous structure. Interestingly, when DIP was added to the polymeric matrix, the diffraction pattern of pure DIP was not detected in the diffractogram of all the 3D-printed samples. This is likely due to the interaction between DIP and TPU, reducing the crystallinity of DIP in the formulation, thus modifying the form from crystalline to amorphous state. These results are consistent with the presence of potential non-covalent interactions reported in the FTIR results.

Thermal analysis was performed to establish the presence of interactions between TPU and DIP. TGA analysis showed that the addition of higher DIP concentrations alters the thermal behaviour of the resulting 3D-printed samples. The T_{onset} of pristine TPU (321 °C) was higher than the T_{onset} for samples containing 10% and 20% of DIP (224 °C and 211 °C, respectively). On the contrary, only a small shift to a lower T_{onset} was found when 5% of DIP was added (316 °C) (Fig. 6D). The lower T_{onset} found for the 3D-printed samples containing 10% and 20% of DIP, even below the pure DIP (284 °C), which is in the crystalline form, suggests that DIP established non-covalent interactions with TPU to form an amorphous solid dispersion. Amorphous drug forms are known to be more reactive than their crystalline counterparts, therefore it is predictable that amorphous forms degrade faster than crystalline forms [72,73]. This therefore explains why DIP degrades at lower temperatures when combined with TPU. It is important to note that the materials described in this work are amorphous solid dispersions. These materials are formed by a drug in its amorphous state dispersed within an excipient matrix [74]. The presence of the polymeric excipient (in this case TPU) in the formulations provides enhanced stability [74]. Therefore, amorphous solid dispersions present higher physicochemical stability than amorphous drugs on its own [74]. This will be an important parameter for the long-term stability of DIP within the grafts. Moreover, TGA results showed that DIP was stable at the temperatures used for the filament preparation and 3D printing process. In order to increase the understanding of these interactions between TPU and DIP, DSC analysis of the 3D-printed samples was also performed (Fig. 6E). The DSC curve for DIP showed the characteristic

DIP melting endothermic peak at 167.5 °C. This melting point was not observed in the TPU-based samples containing DIP. These results suggest that the crystalline drug is converted to the amorphous form after being combined with the TPU matrix. Similar findings have been reported for DIP and different polymer matrices such as poly(caprolactone) (PCL) [21], as well as for other types of drugs such as curcumin [75] or ASA [22]. These results therefore further corroborate the previously stated drug-polymer interactions by FTIR and XRD. Finally, the endothermic peaks found around 213–215 °C for the TPU-based formulations containing 10% and 20% of DIP can be attributed to the faster thermal degradation of these two formulations found in the performed TGA.

Tensile mechanical testing was carried out with 3D-printed samples (Fig. 7A). Fig. 7B shows the values of the elastic modulus obtained for 3D-printed samples containing different amounts of DIP. Interestingly, 3D-printed objects prepared using 5% DIP (w/w) displayed higher stiffness than filaments containing equivalent drug loading ($p < 0.05$). Moreover, 3D-printed samples containing 5% DIP (w/w) displayed higher stiffness than any other 3D-printed sample ($p < 0.05$). This suggest that the presence of 5% of DIP is enhancing the adhesion between layers making the material stiffer. On the other hand, it was observed that increasing DIP loading above 5% (w/w) yielded objects with lower values of elastic modulus ($p < 0.05$). These results indicate that an interaction between DIP and TPU chains is occurring. This is consistent with the previously reported results describing potential interactions between the polymer and the drug observed during thermal analysis and XRD. In addition, these results are consistent with published results which reported that combining polymers with DIP with relative high drug loadings, 20% w/w, for 3D-printed applications can yield objects with lower stiffness [21]. Moreover, when analysing the offset yield strength of the 3D-printed materials (Fig. 7C), a similar trend is observed. However, in this case there are no significant differences between the values obtained for pristine TPU and samples containing 5% DIP (w/w) ($p = 0.885$). The trend observed in these properties is different than the one obtained for the filaments. The only exception is pristine TPU shows no significant differences in the obtained elastic modulus of 3D-printed TPU samples and the elastic modulus of the TPU filaments ($p = 0.816$).

On the other hand, the offset yield strength is affected by the 3D printing technique when comparing the obtained values with the values obtained for the TPU filaments in all cases ($p < 0.05$). These results indicate that drug loading affects the stiffness of the resulting 3D-printed materials. Furthermore, the elastic limit was affected by the 3D-printing technique. It has been reported before that objects prepared using FDM showed lower elastic modulus than objects prepared using injection moulding [76]. This can be attributed to poor attachment between layers and the presence of air-pockets or porous structures between strands [76]. Therefore, it is important to note that printing direction will affect mechanical performance of the resulting materials and needs to be considered when developing new types of medical devices.

The elastic modulus of the 3D-printed samples obtained using TPU-based materials were closer to the elastic modulus of native blood vessels (0.3–1.5 MPa) [77] compared to the elastic modulus

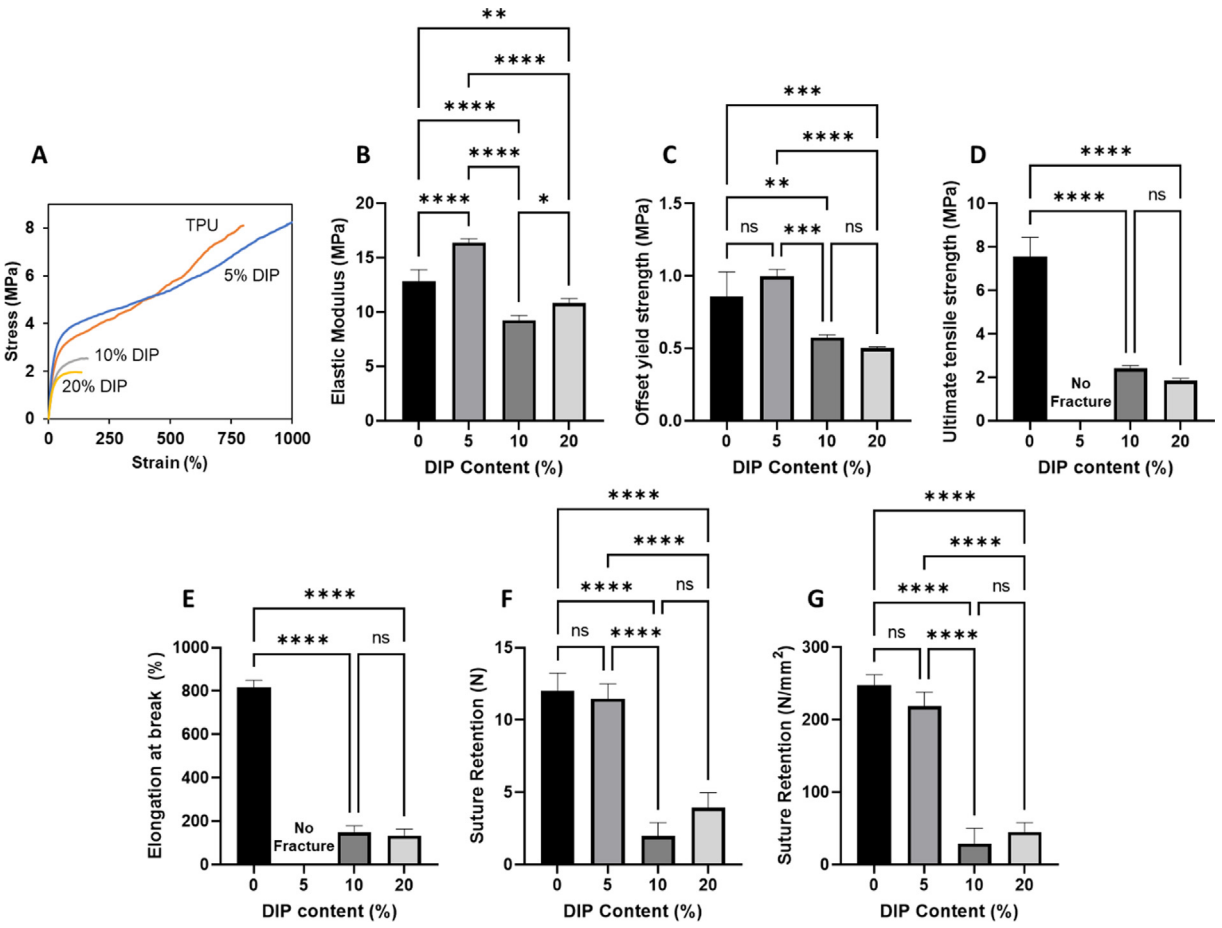

Fig. 7. Representative stress/strain curves for the DIP-loaded 3D-printed samples (A). Elastic modulus (B), offset yield strength (C), ultimate tensile strength (D), elongation at break (E) and suture retention strength (F and G) for the DIP-loaded 3D-printed samples (n = 4).

of synthetic polymers clinically used to prepare vascular grafts such as poly(tetrafluoroethylene) (500 MPa) or Dacron (14,000 MPa) [77,78]. Moreover, elastic modulus of TPU was a closer match to native vessels than other polymers described in the literature such as PCL (ca. 350 MPa), poly(lactic acid) (1–4 GPa), poly(glycolic acid) (7–10 GPa) or poly(lactic-co-glycolic acid) (40–135 MPa) [77]. Moreover, the ultimate tensile strength measured for the TPU-based samples prepared using 3D-printing (Fig. 7D) were within the range of the values obtained for Dacron (around 14 MPa) and native blood vessels (ranging between 1.4 and 11.1 MPa) [77].

The ultimate tensile strength of the resulting materials was evaluated (Fig. 7D). The maximum strain that we could apply with the TA.XTPlus Texture Analyser was 1000%. Interestingly, samples containing 5% DIP (w/w) did not fracture during the test. The stress obtained in these cases ranged between 8 and 9 MPa. Pristine TPU samples and samples containing 10 and 20% (w/w) DIP fractured during the test. These results suggest that the inclusion of 5% DIP (w/w) enhanced the adhesion between layers, yielding a stiffer material. Moreover, samples containing 10 and 20% (w/w) showed significantly lower ultimate tensile strengths ($p < 0.05$). Tensile strengths are lower than Dacron (170–180 MPa) and poly(tetrafluoroethylene) (14 MPa) [77]. However, these values are similar to the ones obtained for biodegradable polymers such as PCL [21] and poly(lactic-co-glycolic acid) [77]. Moreover, these values are aligned with the tensile strengths of blood vessels (1.4–11.1 MPa) [77].

TPU is an elastic material, as observed by the obtained values of the elongation at break (Fig. 7E). As mentioned before, samples containing 5% DIP (w/w) did not fracture during the test (strains up to 1000%). These results indicate that these materials are more elastic than conventional materials used for vascular graft manufacturing or natural blood vessels [78,79]. The elongation at break of the materials containing DIP concentrations higher than 5% (w/w) are lower than the values obtained for pristine TPU. Equivalent results were reported when combining PCL and DIP [21] and biodegradable TPU and DIP [23]. However, these results are similar to the ones obtained for human blood vessels (10–105%) [78].

Suture retention tests were performed using 3D-printed samples (Fig. 7F and G). The results were expressed in "N" and in "N/mm^2" in order to correct deviations due to small differences in sample thickness. However, both type of graphs exhibited the same type of behavior. When 5% (w/w) DIP was incorporated into the material, the suture retention was equivalent to the one obtained for pristine TPU ($p = 0.9028$). However, when DIP concentrations increased above 5% (w/w) the resulting materials showed lower suture retention strength ($p < 0.05$). This behavior has been reported previously for DIP loaded TPU vascular grafts produced using electrospinning [23]. Moreover, the values obtained for the 3D-printed vascular grafts produced using pristine TPU and TPU loaded with 5% (w/w) DIP are higher than the ones reported by Punnakitikashem et al. for the electrospun grafts [23]. Samples with higher DIP concentrations showed a lower suture retention strength than the electrospun materials previously reported in the literature [23]. However, the values of suture retention strength obtained for all the 3D-printed grafts are superior to the ones obtained for human internal mammary artery and human saphenous vein (1–2 N). Accordingly, it can be concluded that the materials developed in this work present higher suture retention strengths than native blood vessels [12].

3.3. In vitro drug release

This assay was performed to evaluate the influence of drug release on antiplatelet activity of 3D-printed materials. The release of DIP from 3D-printed tubular grafts in PBS was evaluated for 30 days (Fig. 8). DIP loaded tubular grafts showed a sustained drug release for 30 days. No obvious burst release was observed within the first 24 h. Tubular grafts containing 5% DIP had a faster release within the first 10 days, which changed to a slow release up to 30 days. However, these two regions were not observed for tubular grafts containing 10% and 20% of DIP. Surprisingly, the total amount of DIP released after 30 days did not increase with drug loading. Although there was a significant increase in the amount of drug released when drug cargo increased from 5% to 10% ($p < 0.05$) after 30 days, no differences were observed when drug loading increased from 10% to 20% ($p > 0.05$). This difference in the release trend can be clearly seen when the release is expressed as percentage of the initial DIP loading. In this case tubular grafts containing 10% DIP showed a higher DIP release (41.07%) when compared to grafts containing 20% DIP (14.13%) ($p < 0.05$) (Fig. 8B). Hence, it can be hypothesised that DIP could be interacting with TPU within the 3D-printed grafts, preventing a higher drug release. This is consistent with the results described in the previous sections. Moreover, these outcomes are aligned with the previous findings reported when combining TPU with DIP or different drugs such as levofloxacin or 17-β-estradiol [23,36,80].

3.4. Platelet adhesion and hemocompatibility of TPU-based 3D-printed samples

PRP was used to measure the platelet deposition on the 3D-printed scaffold surfaces. As previously discussed and reported in the literature, multiple factors such as surface roughness, hydrophilicity and the presence of drug in the surface can influence platelet adhesion [21–23,63–67,81–83]. Fig. 9A-J shows the number and percentage of platelet adhered to the surface of the 3D-printed samples after 2 h and 6 h. Longer periods of time were only evaluated for pristine TPU and 5% DIP samples. Moreover, Fig. 9A-F shows representative SEM images of platelets adhered to the surface of the 3D-printed samples after 2 h and 6 h. Interestingly, materials containing higher DIP loadings (10% and 20%) did not appear to have a more effective antiplatelet activity. In fact, both samples showed a significantly higher number and overall percentage of adhered platelets on their surfaces compared to the pristine TPU and 5% DIP samples ($p < 0.05$). No significant differences were found in the number of platelets adhered to the surface of samples containing 5% DIP and pristine TPU samples ($p = 0.092$). This was due to the enormous difference found in the number of adhered platelets on pristine TPU samples that presented a high variability. This suggests that the presence of DIP does not provide antiplatelet activity to the material for short incubation times (2 h). This test was repeated using 6 h of incubation for the two types of samples. This revealed that 5% DIP had a clear and significant antiplatelet effect when compared to pristine TPU ($p < 0.05$).

TPU and 5% DIP presented equivalent surface properties in terms of wettability and surface roughness (Figs. 4, 5 and 6A). Therefore, the antiplatelet effect can only be attributed to the presence of the drug within the material. This is consistent with previous works describing the impact of DIP loading on antiplatelet properties of materials have been previously reported [21,23]. Interestingly, samples with higher DIP contents (10% and 20%) showed higher platelet adhesion. The explanation for this phenomenon is related to surface properties. It has been previously reported that surface roughness plays a key role on platelet adhesion [63,83]. Pristine TPU and 5% DIP samples had smoother surfaces than samples containing higher DIP loadings (10% and 20%) (Figs. 4 and 5). This led to an increase in the number adhered platelets in the surface of the samples containing 10% and 20% DIP. These results are consistent with the results presented by previous researchers. Linneweber et al. evaluated the effect of the surface roughness on platelet adhesion in impeller-type blood pumps

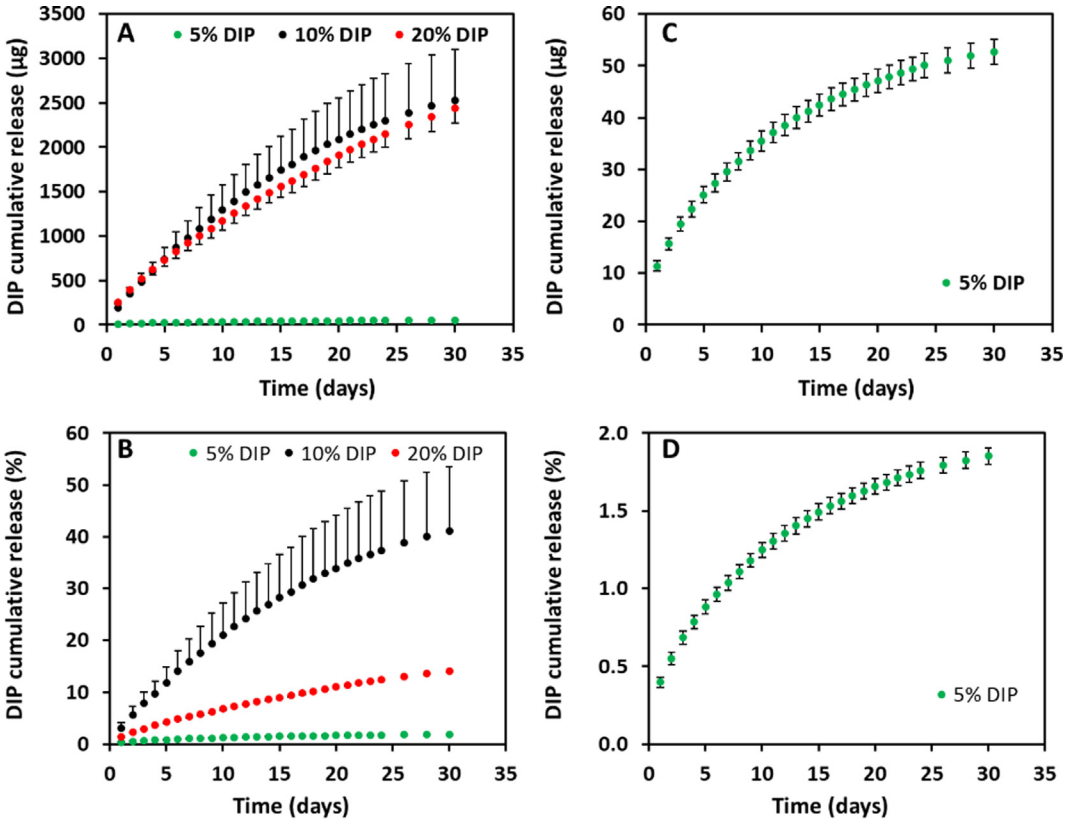

Fig. 8. *In vitro* DIP release curves from DIP-loaded 3D-printed samples up to 30 days in PBS at 37 °C expressed in µg as function of time (A) and expressed in percentage as a function of initial DIP drug loading (B) (n = 4). Figures C and D represent curves of the 5% DIP-loaded 3D-printed samples in a different scale expressed in µg as function of time, and expressed in percentage as a function of initial DIP drug loading, respectively.

manufactured with different surface roughness [82]. They found a positive correlation between the surface irregularities and the number of adherent platelets. In a different study, the authors evaluated the effect of the surface roughness of platelet bags on bacterial and platelet adhesion [83]. Once again, the results showed a positive correlation between platelet adhesion and surface roughness. Moreover, the authors found that not only a higher platelet adhesion and aggregation was observed on rougher surfaces of platelet bags, but also a higher bacterial adhesion and biofilm formation.

It is important to note that surface roughness is not the only parameter that plays a key role on platelet adhesion. Other factors such as surface hydrophilicity also have a critical role in platelet adhesion [66]. Interestingly, samples containing 10 and 20% DIP showed lower surface hydrophilicity than pristine TPU and 5% DIP samples. These results are in correlation with the platelet adhesion results (Fig. 9K). Surface wettability is often considered to explain any differences in the platelet adhesion. However, there is no clear consensus among researchers on what is the role of the hydrophilicity of the materials on platelet adhesion [66]. For instance, a study showed superior performance of diamond-like carbon surface coatings due to its lower hydrophilicity compared to titanium [84]. On the contrary, the higher surface hydrophilicity of the silicon-incorporated, diamond-like carbon films was stated to improve their hemocompatibility [85]. Moreover, zirconium-based amorphous films presenting lower hydrophilicity than pure titanium coatings resulted in a reduction of platelet adhesion [86]. On the other hand, a different study attributed this effect to the high hydrophilicity of functionalized Ti surfaces [87].

It is important to note that in this study no significant differences were found for the contact angle obtained for pristine TPU and 5% DIP samples. However, the later showed a more efficient antiplatelet activity. Overall, it can be concluded that the presence of DIP in the surface is crucial to guarantee antiplatelet activity.

The formulated materials presented in this work are designed for the manufacture of vascular grafts, thus the hemocompatibility of the 3D-printed samples (small 3D-printed disc of 5 mm diameter) was assessed. The hemolysis percentage of all samples was lower than 3% (Fig. 9L). Although the 3D-printed samples without DIP showed the highest hemolysis percentage (2.15 ± 0.66) and the 3D-printed samples containing 20% DIP showed the lowest hemolysis percentage (0.79 ± 0.47), there were no significant differences between the 3D-printed samples ($p > 0.05$). It is important to note that samples showing a hemolysis percentage lower than 5% have been defined as hemocompatible [88].

These results suggest that the ideal material to prepare antiplatelet vascular grafts is TPU containing 5% DIP. Accordingly, the rest of the experiments in this work will be carried out using this type of material.

3.5. *In vitro* cytocompabitility

The biocompatibility of 5% DIP loaded samples was determined through culturing HUVECs onto UV-sterilised samples for a total of 72 h. As seen in Fig. 10A, cells were found to readily attach to both sample types following the initial incubation period of 8 h. Further evaluation at both 24 and 48 h post the attachment period, as can be seen in Fig. 10A, displayed the ability of both samples to support HUVECs adherence. Moreover, the cells adhered to both samples displayed expected endothelial morphology as well typical expression and localisation of CD144, an endothelial specific cell junction marker (Fig. 10B). These images show that the attached cells

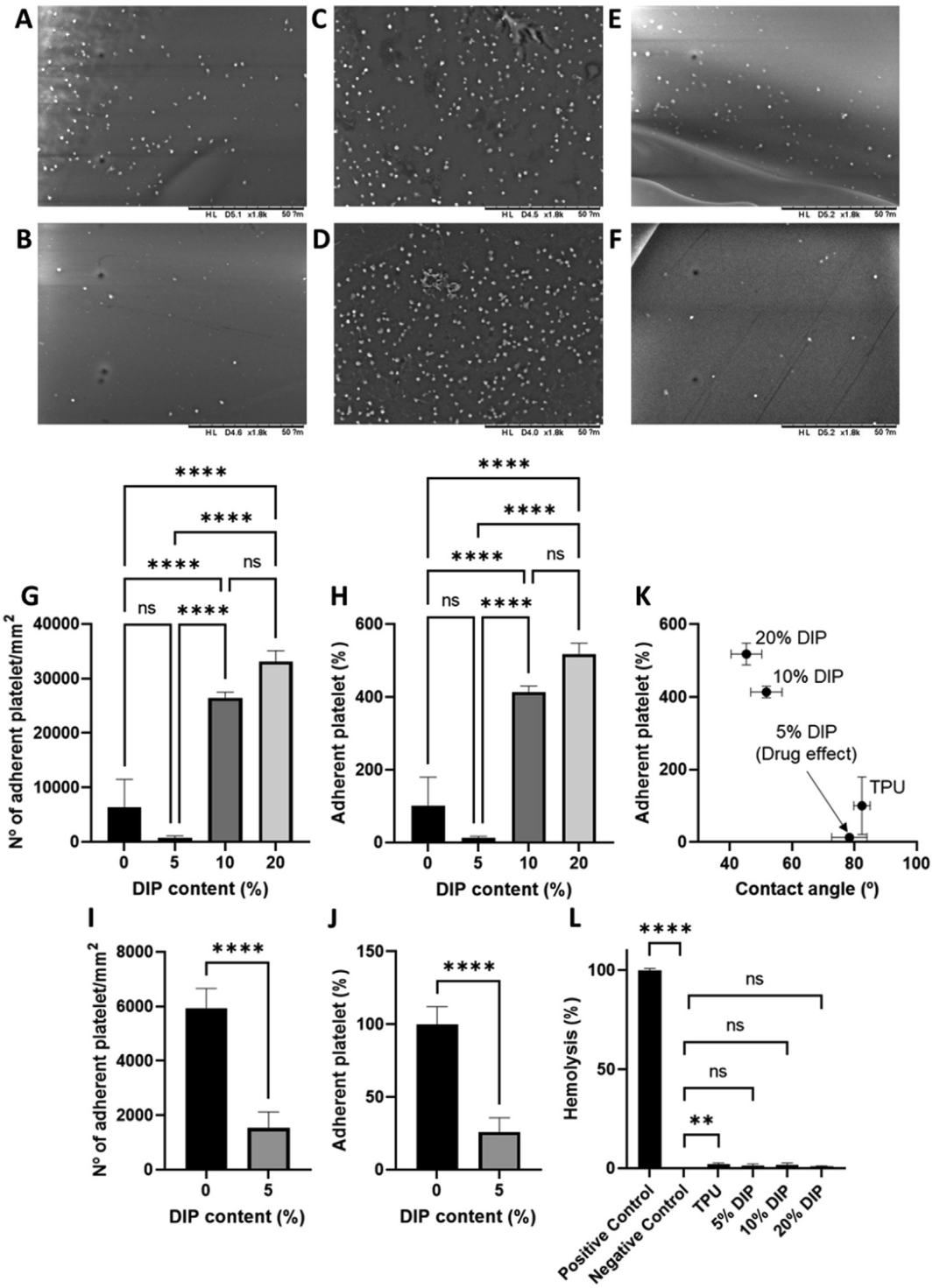

Fig. 9. SEM images of rabbit blood platelet depositions on the surfaces of TPU (A), 5% DIP (B), 10% DIP (C) and 20% DIP-loaded 3D-printed samples (D) after 2 h of incubation time; and TPU (E) and 5% DIP (F) after 6 h of incubation time. Results of the platelet adhesion study expressed in platelet per mm^2 after 2 h (G) and 6 h (I) of incubation time; and expressed in percentage of platelets adhered to the samples surface, using TPU as reference, after 2 h (H) and 6 h (J) of incubation time. Percentage of platelets adhered to the samples surface as a function of the contact angle (K). Rabbit blood hemolysis percentages of the DIP-loaded 3D-printed samples (L) (n = 5).

express CD144 in the correct localisation, highlighting the edges of each cell on top of the 3D-printed samples. Live staining with Vybrant Dil, a live lipophilic membrane stain that diffuses laterally to stain the entire cell, also confirmed the samples to be non-cytotoxic (Fig. 11A). These images show that the cells attached to the scaffolds were functional and alive. Whilst both samples supported cellular attachment and viability, it can be inferred, however, that the sample loaded with 5% DIP provided a more suitable milieu for cellular accommodation as evidenced by the CyQUANT NF cell proliferation assay (Fig. 11B) which observed a statistically significant increase in cell growth between the two assessed timepoints as well as a significantly higher number of cells compared to the TPU control sample at 48 h. Collectively this data confirms the suitability and superiority of the 5% DIP loaded

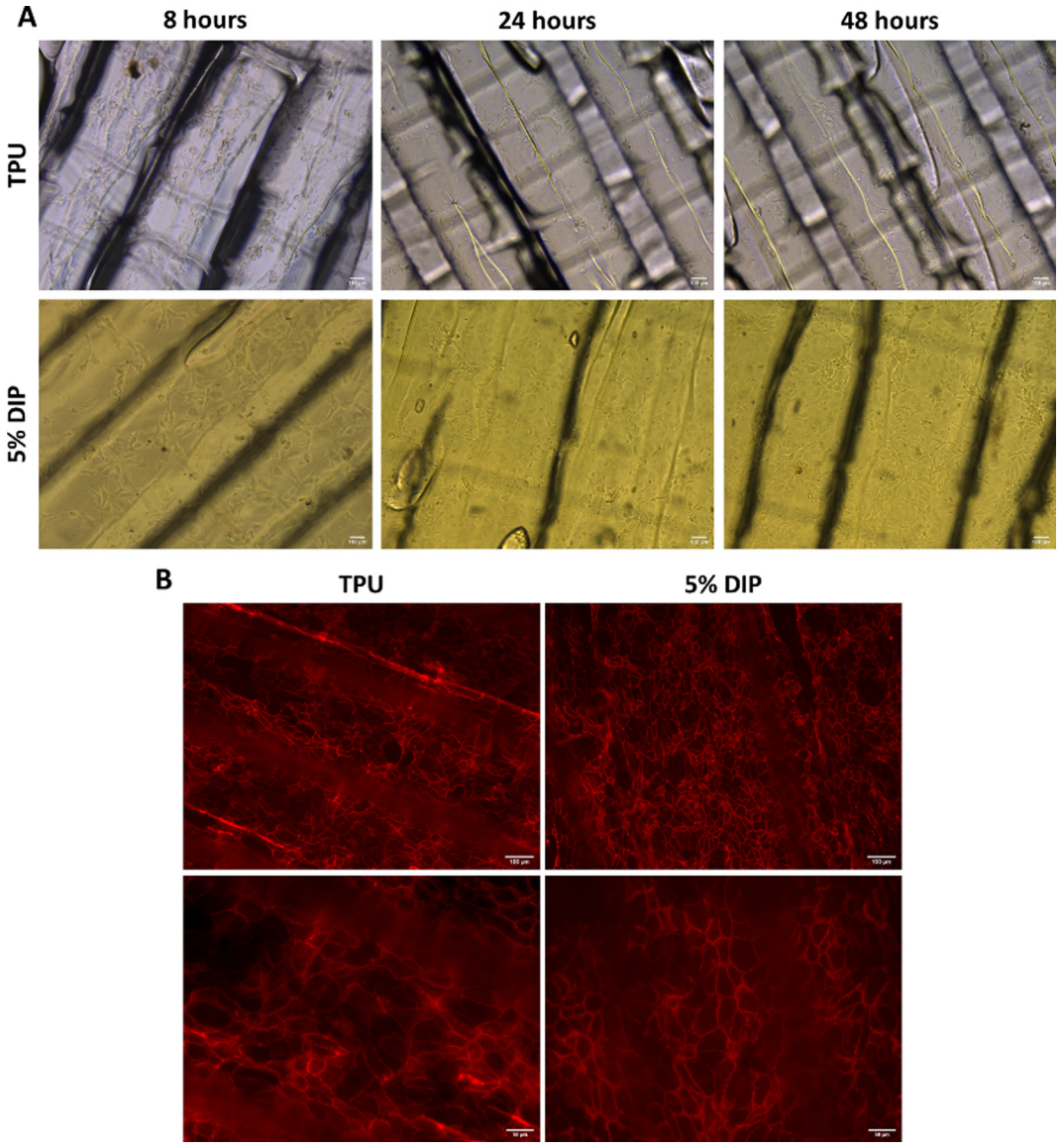

Fig. 10. HUVECs morphology on the surface of TPU and 5% DIP loaded materials 8 h post seeding, 24 and 48 h post attachment. Scale bar = 100 μm (A). Immunofluorescence staining showing that the HUVECs seeded on top of both the TPU and 5% DIP loaded scaffolds expressed the endothelial specific marker CD144, localised to cell–cell junction. Scale bar top panels = 100 μm. Scale bar bottom panels: 50 μm (B).

samples compared to the TPU control samples in supporting an enriching environment for cellular attachment, viability and growth. This is not surprising considering that previous in vitro and in vivo work suggested that DIP stimulates the proliferation of different cell lines including endothelial cells and bone cells [89,90]. However, a previously published work studied the proliferation of HUVEC in contact with TPU containing smaller amounts of DIP (up to 1.5%) [34] suggested that the inclusion of low DIP loadings did not affect cell proliferation. Moreover, PCL 3D-printed samples loaded with 20% (w/w) of DIP did not provided any proliferation improvement over pristine PCL [21]. Cell proliferation therefore not only depends on the DIP content but also the properties of the polymer used to prepare the graft.

The results obtained for the HUVEC cell proliferation in combination with the results obtained for the hemocompatibility test suggest that these materials can have potential for use in biomedical applications. Interestingly, the presence of DIP in the surface of the 3D-printed samples stimulate cell proliferation when compared with a control. We therefore show that the DIP content has a key role in stimulating cell proliferation and so these scaffolds not only have interesting anti-platelet properties but can also be used as scaffolds to support endothelialisation. Graft endothelialisation is a crucial factor implicating the success of vascular prostheses [91]. Endothelialisation should occur in situ to grant effecting and lasting effects. However, in order to maximise the outcomes of this process, cells can be seeded in vitro on the surface of the device prior to implantation to improve the process [91]. The implants described here are ideal candidates for this procedure as endothelial cells can be seeded successfully on the surfaces of the devices while the presence of DIP in the surface promotes their proliferation.

3.6. Versatility of FDM for the development DIP-loaded vascular grafts

FDM is a highly versatile technology that can be used to create a wide variety of geometries. As mentioned before, 3D-printing can

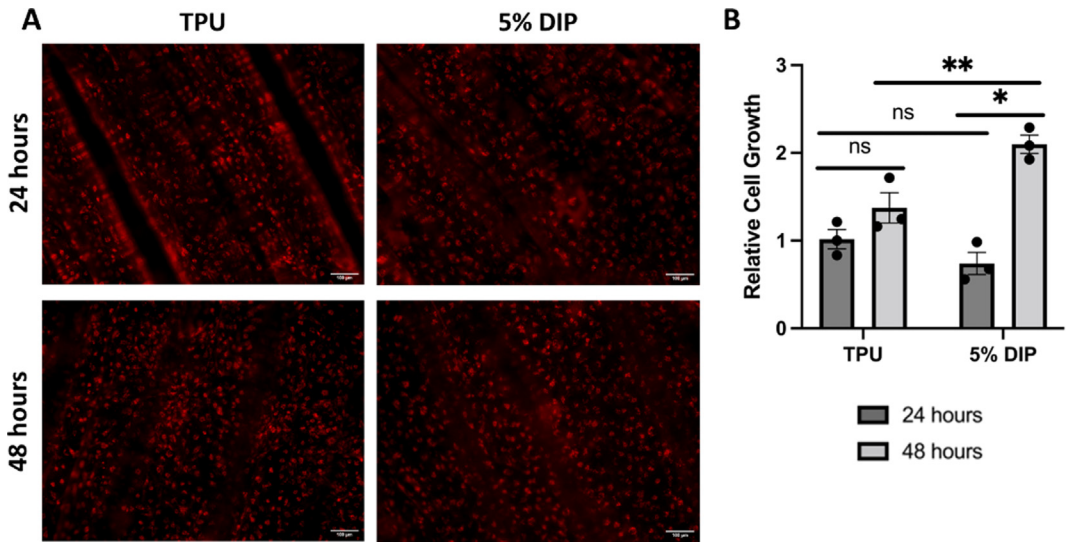

Fig. 11. Live staining with Vybrant™ Dil Stain showed HUVEC viability on the surfaces of both the TPU and 5% DIP loaded samples up to a total of 48 h post attachment. Scale bar = 100 μm (A). HUVEC growth was determined using a CyQUANTTM NF Cell Proliferation Assay for up to a total of 48 h, following a prior 24 h period of time allotted to allow for cellular attachment post seeding. The TPU scaffold without loaded drugs 24 h were set as the control (n = 3). P values are shown: $^{*}p < 0.05$, $^{**}p < 0.01$ (two-tailed *t*-test) (B).

be used to create devices adapted to the anatomy of the patient. Moreover, the versatility of this technology allows for the creation of grafts with enhanced properties. Fig. 12 shows an advanced vascular graft prepared to prevent kinking. Vascular graft kinking can lead to life-threatening stenosis of the graft [92]. This issue can be overcome by adapting the design such as including some reinforce-

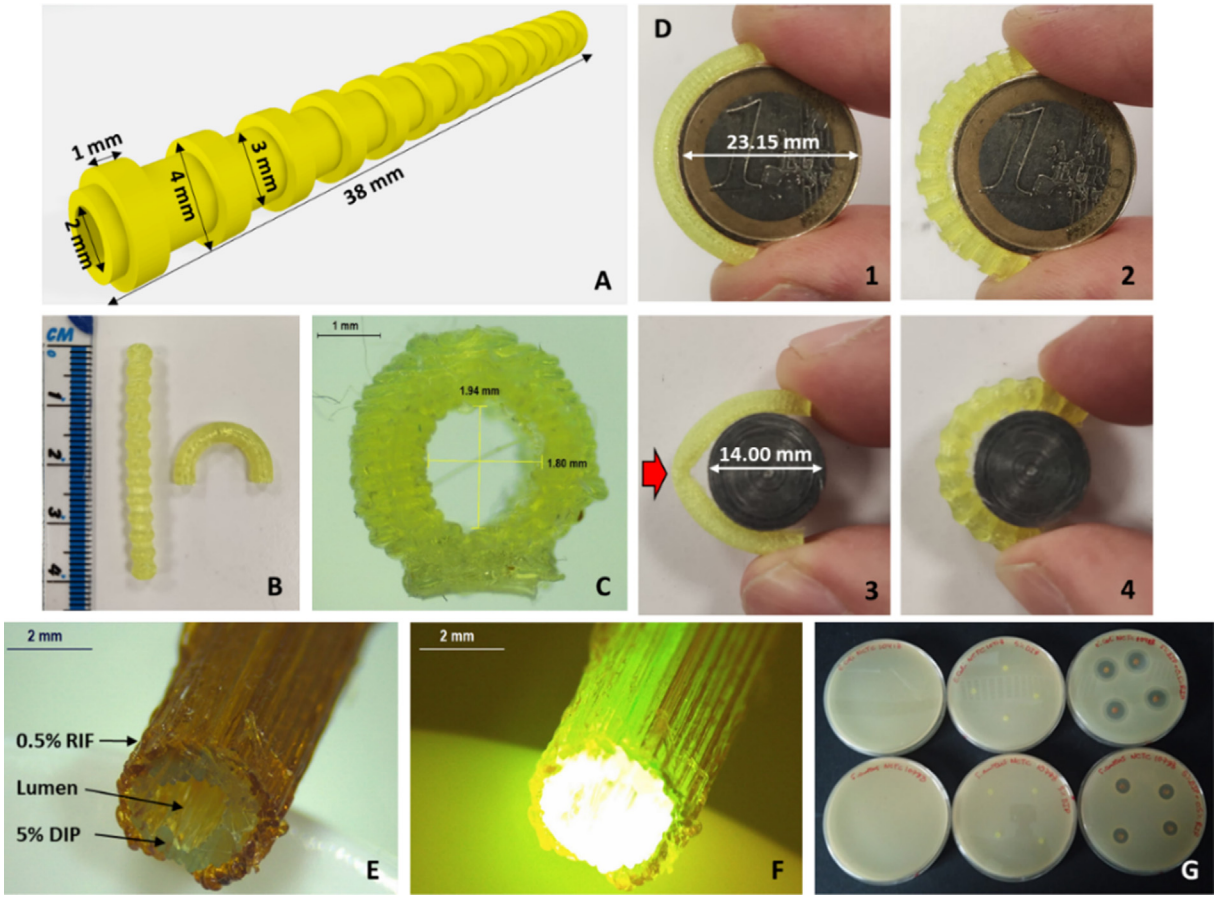

Fig. 12. CAD design of anti-kinking vascular graft (A). Images of anti-kinking vascular graft and curved graft prepared using TPU containing 5% DIP (B). Light microscope image of the cross section of the anti-kinking vascular graft (C). Images showing plain grafts (1 and 3) and anti-kinking grafts (2 and 4) bent around cylindrical objects of different radius (D). Light microscope image of double-layer tubular graft (E) and the same image using the NIGHTSEA Model SFA Stereomicroscope Fluorescence Adapter (F). A picture showing the zones of inhibition obtained for S. aureus and E. coli in MH agar using slices of the double-layer tubular graft (G).

ment rings around the graft to prevent kinking (Fig. 12A) as reported previously [93]. This type of design can be easily printed using FDM as can be seen in Fig. 12B. The CAD design lumen size was 2 mm. Fig. 12C shows that the lumen fidelity was in line with the values obtained for plain vascular grafts.

Plain vascular grafts printed using the 5% DIP TPU filament showed resistance to kinking when the bending radius was ca. 23 mm (Fig. 12D1). These results are superior than previously reported vascular grafts prepared using PCL via-electrospinning [93]. However, when the bending radius was smaller (*ca.* 14 mm) plain grafts bent showing certain degree of kinking (Fig. 12D3). On the other hand, the anti-kinking vascular graft showed superior resistance to kinking even at smaller bending radius (Fig. 12D2 and D4). These results are in line with previously reported anti-kinking grafts prepared using electrospinning using a similar ring design patter [93]. These results indicate that the shape of DIP containing TPU-based vascular graft can be easily adapted. Additionally, the versatility of FDM can be used to change the design of the graft, making it curved to prevent the kinking as shown in the second design presented in Fig. 12B.

In addition to changing the graft geometry, 3D-printed multi-layered objects containing more than one drug prepared using 3D-printing have been previously described as a strategy to improve the adherence to different therapies administered through the oral route [94]. Accordingly, FDM has been used to prepare a graft containing 2 drugs as a proof of concept to demonstrate the versatility of this technique for the preparation of vascular grafts. A concentric bi-layered tubular graft containing DIP in its core and an antibiotic in the outer shell was prepared (Fig. 12E and F). The shell layer was prepared using TPU containing 0.5% RIF. In this case RIF can be used to prevent bacterial infections while DIP will prevent platelet adhesion on the surface of the graft. Moreover, the outer shell prevents DIP release from the outer surface of the graft.

The antimicrobial effect of this samples was tested on bacterial cultures containing *S. aureus* and *E. coli*. Both species are good examples of pathogens that are involved in hospital-associated infections (HAI). The results of the disk diffusion test are displayed in the Fig. 12G. As the inner layer of the double-layer tubular graft was made from the TPU filament containing 5% DIP, tubular grafts containing 5% DIP were employed as a negative control for this experiment. All the double-layer tubular graft samples showed a clear zone of inhibition in both *S. aureus* (11.1 ± 0.2 mm) and *E. coli* (14.1 ± 0.1 mm) plates. Moreover, the tubular grafts containing 5% DIP did not inhibit bacterial growth, indicating the need for such an outer layer to avoid HAI.

Antimicrobial implantable devices using 3D printing technology such as surgical meshes [36,95], dialysis catheters [55,96] or cardiovascular prostheses [22,34], among others, have shown similar results. The use of this double-layer tubular graft can therefore be used to prevent multiple complications of cardiovascular prostheses such as infections and blood clot formation. This strategy can be employed for the manufacture of tubular grafts containing a specific drug located in their lumen while demanding a different drug in the outer part, thus providing an additional function. Additionally, this strategy can be used to avoid drug-drug interactions which can compromise the stability of the device and therapeutic role of the drug components. Moreover, nowadays, competitive prices for dual extrusion fused deposition modelling printers can be found and thus, this technology can be easily transferred and applied in the clinical environment. Finally, it is important to note that FDM technology is versatile and low-cost. Therefore, the translation of this technology to humble clinical setups and research groups could be highly beneficial, this includes the translation of this technology to hospitals and clinical setups in developing countries [31].

4. Conclusions

TPU-based small-diameter cardiovascular grafts containing an antiplatelet drug (DIP) were successfully prepared using FDM. For this purpose, TPU-based filaments loaded with different DIP loadings (up to 20%) were prepared using hot-melt extrusion. These filaments were used in an FDM equipment to prepare different 3D-printed samples. The characterisation of the resulting samples suggested that after the extrusion and printing process the drug present in the samples was in an amorphous state. Moreover, samples printed using filaments loaded with up to 5% (DIP) presented small differences when compared with the original CAD file. On the other hand, objects produced using filaments with higher DIP loading presented a lower level of fidelity.

Mechanical properties of the 3D-printed samples were evaluated. The results suggested that these samples showed comparable mechanical properties than natural blood vessels. Moreover, tubular 3D-printed samples were capable of providing a sustained DIP release for over at least 30 days without displaying any signs of burst release. Interestingly, increasing DIP concentration did not provide a higher drug release. There were no significant differences in the total amount of DIP release after 30 days from samples containing 10 and 20% DIP.

Due to the presence of DIP in the samples, the antiplatelet activity of the materials was evaluated. The results suggested that the samples loaded with 5% DIP presented the highest antiplatelet activity. This may be due to its smoother and more hydrophobic surface. These results therefore indicate that surface roughness and hydrophilicity of the 3D-printed materials has an influence on platelet adhesion. Moreover, these results suggest the smallest DIP loading (5%) was essential to achieving a better antiplatelet activity. Furthermore, all the 3D-printed samples prepared in this work were hemo- and cytocompatible. It is important to note that, the presence of 5% DIP in the samples enhanced the proliferation of HUVEC cells. Combined these results suggest that DIP is an ideal candidate to provide antiplatelet activity and enhance the regeneration of endothelial vascular tissue.

In addition to the use of DIP alone, the use of an FDM-type 3D printer equipped with two extruders was explored to prepare a double-layer tubular graft containing two different drugs (DIP and RIF). This resulted in grafts that exhibited a clear antimicrobial activity against pathogens which are commonly involved in HAI such as *S. aureus* and *E. coli*.

Declaration of Competing Interest

The authors declare that they have no known competing financial interests or personal relationships that could have appeared to influence the work reported in this paper.

Acknowledgements

This work was financially supported by the Wellcome Trust (UNS40040) and the Queen's University Belfast CITI-GENS project funded by the European Union's Horizon 2020 under the Marie Skłodowska-Curie grant agreement [No 945231]. Marc Delgado-Aguilar and Quim Tarrés are Serra Húnter Fellows.

Appendix A. Supplementary material

Supplementary data to this article can be found online at https://doi.org/10.1016/j.matdes.2022.110837.

References

[1] K. Mc Namara, H. Alzubaidi, J.K. Jackson, Cardiovascular disease as a leading cause of death: how are pharmacists getting involved?, Integr Pharm. Res. Pract. 8 (2019) 1–11, https://doi.org/10.2147/IPRP.S133088.

[2] M. Amini, F. Zayeri, M. Salehi, Trend analysis of cardiovascular disease mortality, incidence, and mortality-to-incidence ratio: results from global burden of disease study 2017, BMC Public Health 21 (2021) 401, https://doi.org/10.1186/s12889-021-10429-0.

[3] H. Cui, S. Miao, T. Esworthy, X. Zhou, S. Lee, C. Liu, Z. Yu, J.P. Fisher, M. Mohiuddin, L.G. Zhang, 3D bioprinting for cardiovascular regeneration and pharmacology, Adv. Drug Deliv. Rev. 132 (2018) 252–269, https://doi.org/10.1016/j.addr.2018.07.014.

[4] R.A. Nishimura, C.M. Otto, R.O. Bonow, B.A. Carabello, J.P. Erwin, L.A. Fleisher, H. Jneid, M.J. Mack, C.J. McLeod, P.T. O'Gara, V.H. Rigolin, T.M. Sundt, A. Thompson, 2017 AHA/ACC focused update of the 2014 AHA/ACC Guideline for the management of patients with valvular heart disease: a report of the american college of cardiology/american heart association task force on clinical practice guidelines, Circulation 135 (25) (2017), https://doi.org/10.1161/CIR.0000000000000503.

[5] F.H. Silver, Cardiovascular implants, in: Biomater. Med. Devices Tissue Eng. An Integr. Approach, Springer Netherlands, Dordrecht, 1994, pp. 153–193. <https://doi.org/10.1007/978-94-011-0735-8_5>.

[6] D.W.Y. Toong, H.W. Toh, J.C.K. Ng, P.E.H. Wong, H.L. Leo, S. Venkatraman, L.P. Tan, H.Y. Ang, Y. Huang, Bioresorbable polymeric scaffold in cardiovascular applications, Int. J. Mol. Sci. 21 (2020) 3444, https://doi.org/10.3390/ijms21103444.

[7] Q.A. Majid, A.T.R. Fricker, D.A. Gregory, N. Davidenko, O. Hernandez Cruz, R.J. Jabbour, T.J. Owen, P. Basnett, B. Lukasiewicz, M. Stevens, S. Best, R. Cameron, S. Sinha, S.E. Harding, I. Roy, Natural biomaterials for cardiac tissue engineering: a highly biocompatible solution, Nat. Biomater. Cardiac Tissue Eng.: Highly Biocompat. Sol., Front. Cardiovasc. Med. 7 (2020), https://doi.org/10.3389/fcvm.2020.554597.

[8] S. Park, J. Kim, M.-K. Lee, C. Park, H.-D. Jung, H.-E. Kim, T.-S. Jang, Fabrication of strong, bioactive vascular grafts with PCL/collagen and PCL/silica bilayers for small-diameter vascular applications, Mater. Des. 181 (2019) 108079, https://doi.org/10.1016/j.matdes.2019.108079.

[9] T. Wang, N. Dong, H. Yan, S.Y. Wong, W. Zhao, K. Xu, D. Wang, S. Li, X. Qiu, Regeneration of a neoartery through a completely autologous acellular conduit in a minipig model: a pilot study, J. Transl. Med. 17 (2019) 24, https://doi.org/10.1186/s12967-018-1763-5.

[10] P. Mallis, A. Kostakis, C. Stavropoulos-Giokas, E. Michalopoulos, Future perspectives in small-diameter vascular graft engineering, Bioengineering. 7 (2020) 160, https://doi.org/10.3390/bioengineering7040160.

[11] D. Jin, S. Wu, H. Kuang, P. Zhang, M. Yin, Preliminary application of a cell-free mono-layered vascular scaffold in a rabbit model, Mater. Des. 198 (2021) 109301, https://doi.org/10.1016/j.matdes.2020.109301.

[12] F. Zhang, Y.u. Xie, H. Celik, O. Akkus, S.H. Bernacki, M.W. King, Engineering small-caliber vascular grafts from collagen filaments and nanofibers with comparable mechanical properties to native vessels, Biofabrication. 11 (3) (2019) 035020, https://doi.org/10.1088/1758-5090/ab15ce.

[13] S. Ravi, E.L. Chaikof, Biomaterials for vascular tissue engineering, Regen. Med. 5 (1) (2010) 107–120, https://doi.org/10.2217/rme.09.77.

[14] D. Chen, L. Zhang, W. Zhang, Z. Tang, W. Fu, R. Hu, B. Feng, H. Hong, H. Zhang, Shapeable large-pore electrospun polycaprolactam cotton facilitates the rapid formation of a functional tissue engineered vascular graft, Mater. Des. 191 (2020) 108631, https://doi.org/10.1016/j.matdes.2020.108631.

[15] I. Skovrind, E.B. Harvald, H. Juul Belling, C.D. Jørgensen, J.S. Lindholt, D.C. Andersen, Concise Review: Patency of Small-Diameter Tissue-Engineered Vascular Grafts: A Meta-Analysis of Preclinical Trials, Stem Cells Transl. Med. (2019) sctm.18-0287. <https://doi.org/10.1002/sctm.18-0287>.

[16] J.D. Kakisis, C.D. Liapis, C. Breuer, B.E. Sumpio, Artificial blood vessel: the Holy Grail of peripheral vascular surgery, J. Vasc. Surg. 41 (2) (2005) 349–354, https://doi.org/10.1016/j.jvs.2004.12.026.

[17] A. Cafarelli, P. Losi, A.R. Salgarella, M.C. Barsotti, I.B. Di Cioccio, I. Foffa, L. Vannozzi, P. Pingue, G. Soldani, L. Ricotti, Small-caliber vascular grafts based on a piezoelectric nanocomposite elastomer: mechanical properties and biocompatibility, J. Mech. Behav. Biomed. Mater. 97 (2019) 138–148, https://doi.org/10.1016/j.jmbbm.2019.05.017.

[18] F.O. Obiweluozor, G.A. Emechebe, D.-W. Kim, H.-J. Cho, C.H. Park, C.S. Kim, I.S. Jeong, Considerations in the development of small-diameter vascular graft as an alternative for bypass and reconstructive surgeries: a review, cardiovasc, Eng. Technol. 11 (5) (2020) 495–521, https://doi.org/10.1007/s13239-020-00482-y.

[19] J. Han, P.I. Lelkes, Drug-eluting vascular grafts, 2014, pp. 405–427. <https://doi.org/10.1007/978-1-4614-9434-8_19>.

[20] M. Rychter, A. Baranowska-Korczyc, B. Milanowski, M. Jarek, B.M. Maciejewska, E.L. Coy, J. Lulek, Cilostazol-loaded poly(ε-caprolactone) electrospun drug delivery system for cardiovascular applications, Pharm. Res. 35 (2018) 32, https://doi.org/10.1007/s11095-017-2314-0.

[21] J. Domínguez-Robles, T. Shen, V.A. Cornelius, F. Corduas, E. Mancuso, R.F. Donnelly, A. Margariti, D.A. Lamprou, E. Larrañeta, Development of drug loaded cardiovascular prosthesis for thrombosis prevention using 3D printing, Mater. Sci. Eng. C. 129 (2021) 112375, https://doi.org/10.1016/j.msec.2021.112375.

[22] J. Domínguez-Robles, L. Diaz-Gomez, E. Utomo, T. Shen, C.J. Picco, C. Alvarez-Lorenzo, A. Concheiro, R.F. Donnelly, E. Larrañeta, Use of 3D printing for the development of biodegradable antiplatelet materials for cardiovascular applications, Pharmaceuticals 14 (2021) 921, https://doi.org/10.3390/ph14090921.

[23] P. Punnakitikashem, D. Truong, J.U. Menon, K.T. Nguyen, Y.i. Hong, Electrospun biodegradable elastic polyurethane scaffolds with dipyridamole release for small diameter vascular grafts, Acta Biomater. 10 (11) (2014) 4618–4628, https://doi.org/10.1016/j.actbio.2014.07.031.

[24] D. Kim, J.J. Chung, Y. Jung, S.H. Kim, The effect of Substance P/Heparin conjugated PLCL polymer coating of bioinert ePTFE vascular grafts on the recruitment of both ECs and SMCs for accelerated regeneration, Sci. Rep. 9 (2019) 17083, https://doi.org/10.1038/s41598-019-53514-6.

[25] M. Carrabba, P. Madeddu, Current strategies for the manufacture of small size tissue engineering vascular grafts, Front. Bioeng. Biotechnol. 6 (2018), https://doi.org/10.3389/fbioe.2018.00041.

[26] T.D. Ngo, A. Kashani, G. Imbalzano, K.T.Q. Nguyen, D. Hui, Additive manufacturing (3D printing): a review of materials, methods, applications and challenges, Compos. Part B Eng. 143 (2018) 172–196, https://doi.org/10.1016/j.compositesb.2018.02.012.

[27] F.M. Mwema, E.T. Akinlabi, Basics of Fused Deposition Modelling (FDM), 2020, pp. 1–15. <https://doi.org/10.1007/978-3-030-48259-6_1>.

[28] S. Kholgh Eshkalak, E. Rezvani Ghomi, Y. Dai, D. Choudhury, S. Ramakrishna, The role of three-dimensional printing in healthcare and medicine, Mater. Des. 194 (2020) 108940, https://doi.org/10.1016/j.matdes.2020.108940.

[29] P. Awasthi, S.S. Banerjee, Fused deposition modeling of thermoplastic elastomeric materials: Challenges and opportunities, Addit. Manuf. 46 (2021) 102177, https://doi.org/10.1016/j.addma.2021.102177.

[30] A.M.S. Ibrahim, R.R. Jose, A.N. Rabie, T.L. Gerstle, B.T. Lee, S.J. Lin, Three-dimensional printing in developing countries, Plast. Reconstr. Surg. - Glob. Open. 3 (7) (2015) e443, https://doi.org/10.1097/GOX.0000000000000298.

[31] J.S. Cuellar, G. Smit, A.A. Zadpoor, P. Breedveld, Ten guidelines for the design of non-assembly mechanisms: the case of 3D-printed prosthetic hands, Proc. Inst. Mech. Eng. Part H J. Eng. Med. 232 (9) (2018) 962–971, https://doi.org/10.1177/0954411918794734.

[32] B. Shaqour, A. Samaro, B. Verleije, K. Beyers, C. Vervaet, P. Cos, Production of drug delivery systems using fused filament fabrication: a systematic review, Pharmaceutics 12 (2020) 517, https://doi.org/10.3390/pharmaceutics12060517.

[33] A. Goyanes, F. Fina, A. Martorana, D. Sedough, S. Gaisford, A.W. Basit, Development of modified release 3D printed tablets (printlets) with pharmaceutical excipients using additive manufacturing, Int. J. Pharm. 527 (1-2) (2017) 21–30, https://doi.org/10.1016/j.ijpharm.2017.05.021.

[34] N.K. Martin, J. Domínguez-Robles, S.A. Stewart, V.A. Cornelius, Q.K. Anjani, E. Utomo, I. García-Romero, R.F. Donnelly, A. Margariti, D.A. Lamprou, E. Larrañeta, Fused deposition modelling for the development of drug loaded cardiovascular prosthesis, Int. J. Pharm. 595 (2021) 120243, https://doi.org/10.1016/j.ijpharm.2021.120243.

[35] S. Stewart, J. Domínguez-Robles, V. McIlorum, E. Mancuso, D. Lamprou, R. Donnelly, E. Larrañeta, Development of a biodegradable subcutaneous implant for prolonged drug delivery using 3D printing, Pharmaceutics 12 (2020) 105, https://doi.org/10.3390/pharmaceutics12020105.

[36] J. Domínguez-Robles, C. Mancinelli, E. Mancuso, I. García-Romero, B.F. Gilmore, L. Casettari, E. Larrañeta, D.A. Lamprou, 3D printing of drug-loaded thermoplastic polyurethane meshes: a potential material for soft tissue reinforcement in vaginal surgery, Pharmaceutics 12 (2020) 63, https://doi.org/10.3390/pharmaceutics12010063.

[37] Y. Ghantous, A. Nashef, A. Mohanna, I. Abu-El-naaj, Three-dimensional technology applications in maxillofacial reconstructive surgery: current surgical implications, Nanomaterials. 10 (2020) 2523, https://doi.org/10.3390/nano10122523.

[38] J. Domínguez-Robles, N. Martin, M. Fong, S. Stewart, N. Irwin, M. Rial-Hermida, R. Donnelly, E. Larrañeta, Antioxidant PLA composites containing lignin for 3D printing applications: a potential material for healthcare applications, Pharmaceutics 11 (2019) 165, https://doi.org/10.3390/pharmaceutics11040165.

[39] P.K. Penumakala, J. Santo, A. Thomas, A critical review on the fused deposition modeling of thermoplastic polymer composites, Compos. Part B Eng. 201 (2020) 108336, https://doi.org/10.1016/j.compositesb.2020.108336.

[40] R. Al Nakib, A. Toncheva, V. Fontaine, J. Vanheuverzwijn, J.-M. Raquez, F. Meyer, Thermoplastic polyurethanes for biomedical application: a synthetic, mechanical, antibacterial, and cytotoxic study, J. Appl. Polym. Sci. 139 (4) (2022) 51666, https://doi.org/10.1002/app.v139.410.1002/app.51666.

[41] S. Wendels, L. Avérous, Biobased polyurethanes for biomedical applications, Bioact. Mater. 6 (4) (2021) 1083–1106, https://doi.org/10.1016/j.bioactmat.2020.10.002.

[42] J. Xiao, Y. Gao, The manufacture of 3D printing of medical grade TPU, Prog. Addit. Manuf. 2 (3) (2017) 117–123, https://doi.org/10.1007/s40964-017-0023-1.

[43] Lubrizol, Polymers for Cardiology Applications, 2021. <https://www.lubrizol.com/Health/Medical/Markets/Cardiology> (Accessed October 8, 2021).

[44] J.A. Weisman, J.C. Nicholson, K. Tappa, U. Jammalamadaka, C.G. Wilson, D.K. Mills, Antibiotic and chemotherapeutic enhanced three-dimensional printer filaments and constructs for biomedical applications, Int. J. Nanomed. 10 (2015) 357–370, https://doi.org/10.2147/IJN.S74811 [doi].

[45] S.A. Stewart, J. Domínguez-Robles, V.J. McIlorum, Z. Gonzalez, E. Utomo, E. Mancuso, D.A. Lamprou, R.F. Donnelly, E. Larrañeta, Poly(caprolactone)-based coatings on 3D-printed biodegradable implants: a novel strategy to prolong delivery of hydrophilic drugs, Mol. Pharm. 17 (9) (2020) 3487–3500, https://doi.org/10.1021/acs.molpharmaceut.0c00515.
[46] J. Dominguez-Robles, S.A. Stewart, A. Rendl, Z. Gonzalez, R.F. Donnelly, E. Larraneta, Lignin and cellulose blends as pharmaceutical excipient for tablet manufacturing via direct compression, Biomolecules 9 (2019), https://doi.org/10.3390/biom9090423. https://doi.org/E423 [pii].
[47] X. Hou, W. Zheng, V. Kodur, H. Sun, Effect of temperature on mechanical properties of prestressing bars, Constr. Build. Mater. 61 (2014) 24–32, https://doi.org/10.1016/j.conbuildmat.2014.03.001.
[48] J.S. Afonso, P.A.L.S. Martins, M.J.B.C. Girao, R.M. Natal Jorge, A.J.M. Ferreira, T. Mascarenhas, A.A. Fernandes, J. Bernardes, E.C. Baracat, G. Rodrigues de Lima, B. Patricio, Mechanical properties of polypropylene mesh used in pelvic floor repair, Int. Urogynecol. J. 19 (3) (2008) 375–380, https://doi.org/10.1007/s00192-007-0446-1.
[49] K.A. McKenna, M.T. Hinds, R.C. Sarao, P.-C. Wu, C.L. Maslen, R.W. Glanville, D. Babcock, K.W. Gregory, Mechanical property characterization of electrospun recombinant human tropoelastin for vascular graft biomaterials, Acta Biomater. 8 (1) (2012) 225–233, https://doi.org/10.1016/j.actbio.2011.08.001.
[50] K. McAvoy, D. Jones, R.R.S. Thakur, Synthesis and Characterisation of Photocrosslinked poly(ethylene glycol) diacrylate Implants for Sustained Ocular Drug Delivery, Pharm. Res. 35 (2018) 36, https://doi.org/10.1007/s11095-017-2298-9.
[51] M. Samie, M.A. Yameen, H.F. Ikram, H. Iqbal, A.A. Chaudhry, I. ur Rehman, A.F. Khan, Fabrication of dual drug loaded bilayered chitosan based composite scaffolds as osteochondral substitutes and evaluation of in vitro cell response using the MC3T3 pre-osteoblast cell line, Cellulose 27 (4) (2020) 2253–2266, https://doi.org/10.1007/s10570-019-02915-x.
[52] J. Dey, H. Xu, J. Shen, P. Thevenot, S.R. Gondi, K.T. Nguyen, B.S. Sumerlin, L. Tang, J. Yang, Development of biodegradable crosslinked urethane-doped polyester elastomers, Biomaterials 29 (35) (2008) 4637–4649, https://doi.org/10.1016/j.biomaterials.2008.08.020.
[53] S. Haghjooy Javanmard, J. Anari, A. Zargar Kharazi, E. Vatankhah, In vitro hemocompatibility and cytocompatibility of a three-layered vascular scaffold fabricated by sequential electrospinning of PCL, collagen, and PLLA nanofibers, J. Biomater. Appl. 31 (2016) 438–449, https://doi.org/10.1177/0885328216652068.
[54] A. Balaji, S.K. Jaganathan, A.F. Ismail, R. Rajasekar, Fabrication and hemocompatibility assessment of novel polyurethane-based bio-nanofibrous dressing loaded with honey and Carica papaya extract for the management of burn injuries, Int. J. Nanomed. 11 (2016) 4339–4355.
[55] E. Mathew, J. Domínguez-Robles, S.A. Stewart, E. Mancuso, K. O'Donnell, E. Larrañeta, D.A. Lamprou, Fused deposition modeling as an effective tool for anti-infective dialysis catheter fabrication, ACS Biomater. Sci. Eng. 5 (11) (2019) 6300–6310, https://doi.org/10.1021/acsbiomaterials.9b0118510.1021/acsbiomaterials.9b01185.s001.
[56] M. Alshafiee, M.K. Aljammal, D. Markl, A. Ward, K. Walton, L. Blunt, S. Korde, S. K. Pagire, A.L. Kelly, A. Paradkar, B.R. Conway, K. Asare-Addo, Hot-melt extrusion process impact on polymer choice of glyburide solid dispersions: the effect of wettability and dissolution, Int. J. Pharm. 559 (2019) 245–254, https://doi.org/10.1016/j.ijpharm.2019.01.038.
[57] G. Verstraete, A. Samaro, W. Grymonpré, V. Vanhoorne, B. Van Snick, M.N. Boone, T. Hellemans, L. Van Hoorebeke, J.P. Remon, C. Vervaet, 3D printing of high drug loaded dosage forms using thermoplastic polyurethanes, Int. J. Pharm. 536 (1) (2018) 318–325, https://doi.org/10.1016/j.ijpharm.2017.12.002.
[58] A. Repanas, B. Glasmacher, Dipyridamole embedded in Polycaprolactone fibers prepared by coaxial electrospinning as a novel drug delivery system, J. Drug Deliv. Sci. Technol. 29 (2015) 132–142, https://doi.org/10.1016/j.jddst.2015.07.001.
[59] G. Caiti, J.G.G. Dobbe, G.J. Strijkers, S.D. Strackee, G.J. Streekstra, Positioning error of custom 3D-printed surgical guides for the radius: influence of fitting location and guide design, Int. J. Comput. Assist. Radiol. Surg. 13 (4) (2018) 507–518, https://doi.org/10.1007/s11548-017-1682-6.
[60] I. Seoane-Viaño, P. Januskaite, C. Alvarez-Lorenzo, A.W. Basit, A. Goyanes, Semi-solid extrusion 3D printing in drug delivery and biomedicine: personalised solutions for healthcare challenges, J. Control. Release. 332 (2021) 367–389, https://doi.org/10.1016/j.jconrel.2021.02.027.
[61] C.J. Picco, J. Domínguez-Robles, E. Utomo, A.J. Paredes, F. Volpe-Zanutto, D. Malinova, R.F. Donnelly, E. Larrañeta, 3D-printed implantable devices with biodegradable rate-controlling membrane for sustained delivery of hydrophobic drugs, Drug Deliv. 29 (1) (2022) 1038–1048, https://doi.org/10.1080/10717544.2022.2057620.
[62] J. Qin, Y. Jiang, J. Fu, Y. Wan, R. Yang, W. Gao, H. Wang, Evaluation of drug release property and blood compatibility of aspirin-loaded electrospun PLA/RSF composite nanofibers, Iran. Polym. J. 22 (10) (2013) 729–737, https://doi.org/10.1007/s13726-013-0171-1.
[63] W. van Oeveren, Obstacles in Haemocompatibility Testing, Scientifica (Cairo). 2013 (2013) 1–14, https://doi.org/10.1155/2013/392584.
[64] J.M. Schmehl, C. Harder, H.P. Wendel, C.D. Claussen, G. Tepe, Silicon carbide coating of nitinol stents to increase antithrombogenic properties and reduce nickel release, Cardiovasc. Revascularization Med. 9 (4) (2008) 255–262.
[65] S. Beumer, H.F. Heijnen, M. IJsseldijk, E. Orlando, P. de Groot, J. Sixma, Platelet adhesion to fibronectin in flow: the importance of von Willebrand factor and glycoprotein Ib, Blood. 86 (1995) 3452–3460.
[66] M. Cihova, E. Müller, Y. Chandorkar, K. Thorwarth, G. Fortunato, K. Maniura-Weber, J.F. Löffler, M. Rottmar, Palladium-based metallic glass with high thrombogenic resistance for blood-contacting medical devices, Adv. Funct. Mater. 32 (4) (2022) 2108256, https://doi.org/10.1002/adfm.v32.410.1002/adfm.202108256.
[67] H.T. Spijker, R. Bos, H.J. Busscher, R. Graaff, W. Van Oeveren, Adhesion of blood platelets under flow to wettability gradient polyethylene surfaces made in a shielded gas plasma, J. Adhes. Sci. Technol. 16 (13) (2002) 1703–1713, https://doi.org/10.1163/156856102320396094.
[68] Y.B.J. Aldenhoff, R. Blezer, T. Lindhout, L.H. Koole, Photo-immobilization of dipyridamole (Persantin®) at the surface of polyurethane biomaterials: reduction ofin vitro thrombogenicity, Biomaterials 18 (2) (1997) 167–172, https://doi.org/10.1016/S0142-9612(96)00095-6.
[69] V. Bakola, V. Karagkiozaki, A.R. Tsiapla, F. Pappa, I. Moutsios, E. Pavlidou, S. Logothetidis, Dipyridamole-loaded biodegradable PLA nanoplatforms as coatings for cardiovascular stents, Nanotechnology 29 (27) (2018) 275101, https://doi.org/10.1088/1361-6528/aabc69.
[70] M. Silva Oliveira, S.C. Miguel Agustinho, A.M.d. Guzzi Plepis, M. Tabak, On the thermal decomposition of dipyridamole: thermogravimetric, differential scanning calorimetric and spectroscopic studies, Spectrosc. Lett. 39 (2) (2006) 145–161, https://doi.org/10.1080/00387010500531126.
[71] BASF, Elastollan Thermoplastic Polyurethane, (n.d.).
[72] D.E. Moseson, M.A. Jordan, D.D. Shah, I.D. Corum, B.R. Alvarenga Jr., L.S. Taylor, Application and limitations of thermogravimetric analysis to delineate the hot melt extrusion chemical stability processing window, Int. J. Pharm. 590 (2020) 119916, https://doi.org/10.1016/j.ijpharm.2020.119916.
[73] S.R. Byrn, W. Xu, A.W. Newman, Chemical reactivity in solid-state pharmaceuticals: formulation implications, Adv. Drug Deliv. Rev. 48 (1) (2001) 115–136, https://doi.org/10.1016/S0169-409X(01)00102-8.
[74] S. V. Bhujbal, B. Mitra, U. Jain, Y. Gong, A. Agrawal, S. Karki, L.S. Taylor, S. Kumar, Q. (Tony) Zhou, Pharmaceutical amorphous solid dispersion: a review of manufacturing strategies, Acta Pharm. Sin. B. 11 (2021) 2505–2536. <https://doi.org/10.1016/j.apsb.2021.05.014>.
[75] E. Larrañeta, M. Imízcoz, J.X. Toh, N.J. Irwin, A. Ripolin, A. Perminova, J. Domínguez-Robles, A. Rodríguez, R.F. Donnelly, Synthesis and characterization of lignin hydrogels for potential applications as drug eluting antimicrobial coatings for medical materials, ACS Sustain. Chem. Eng. 6 (7) (2018) 9037–9046, https://doi.org/10.1021/acssuschemeng.8b0137110.1021/acssuschemeng.8b01371.s001.
[76] M. Lay, N.L.N. Thajudin, Z.A.A. Hamid, A. Rusli, M.K. Abdullah, R.K. Shuib, Comparison of physical and mechanical properties of PLA, ABS and nylon 6 fabricated using fused deposition modeling and injection molding, Compos. Part B Eng. 176 (2019) 107341, https://doi.org/10.1016/j.compositesb:2019.107341.
[77] M.A. Hiob, S. She, L.D. Muiznieks, A.S. Weiss, Biomaterials and modifications in the development of small-diameter vascular grafts, ACS Biomater. Sci. Eng. 3 (5) (2017) 712–723, https://doi.org/10.1021/acsbiomaterials.6b00220.
[78] W.E. King, B.A. Minden-Birkenmaier, G.L. Bowlin, Synthetic Materials: Processing and Surface Modifications for Vascular Tissue Engineering, in: Tissue-Engineered Vasc. Grafts, Springer International Publishing, Cham, 2020, pp. 137–186. <https://doi.org/10.1007/978-3-030-05336-9_2>.
[79] H. Ye, K. Zhang, D. Kai, Z. Li, X.J. Loh, Polyester elastomers for soft tissue engineering, Chem. Soc. Rev. 47 (12) (2018) 4545–4580, https://doi.org/10.1039/C8CS00161H.
[80] Z.-L. Farmer, E. Utomo, J. Domínguez-Robles, C. Mancinelli, E. Mathew, E. Larrañeta, D.A. Lamprou, 3D printed estradiol-eluting urogynecological mesh implants: influence of material and mesh geometry on their mechanical properties, Int. J. Pharm. 593 (2021) 120145, https://doi.org/10.1016/j.ijpharm.2020.120145.
[81] NANAE Tsunoda, KEN.-ICHI. Kokubo, KIYOTAKA Sakai, MAKOTO Fukuda, MAKOTO Miyazaki, TATSUO Hiyoshi, Surface roughness of cellulose hollow fiber dialysis membranes and platelet adhesion, ASAIO J. 45 (5) (1999) 418–423.
[82] J. Linneweber, P.M. Dohmen, U. Kerzscher, K. Affeld, Y. Nosé, W. Konertz, The effect of surface roughness on activation of the coagulation system and platelet adhesion in rotary blood pumps, Artif. Organs. 31 (5) (2007) 345–351, https://doi.org/10.1111/j.1525-1594.2007.00391.x.
[83] N. Hadjesfandiari, P. Schubert, S. Fallah Toosi, Z. Chen, B. Culibrk, S. Ramirez-Arcos, D.V. Devine, D.E. Brooks, Effect of texture of platelet bags on bacterial and platelet adhesion, Transfusion 56 (11) (2016) 2808–2818, https://doi.org/10.1111/trf.13756.
[84] M.I. Jones, I.R. McColl, D.M. Grant, K.G. Parker, T.L. Parker, Protein adsorption and platelet attachment and activation, on TiN, TiC, and DLC coatings on titanium for cardiovascular applications, J. Biomed. Mater. Res. 52 (2000) 413–421, https://doi.org/10.1002/1097-4636(200011)52:2<413::AID-JBM23>3.0.CO;2-U.
[85] R. Roy, H. Choi, J. Yi, M. Moon, K. Lee, D. Han, J. Shin, A. Kamijo, T. Hasebe, Hemocompatibility of surface-modified, silicon-incorporated, diamond-like carbon films, Acta Biomater. 5 (1) (2009) 249–256, https://doi.org/10.1016/j.actbio.2008.07.031.
[86] C.-H. Chang, C.-L. Li, C.-C. Yu, Y.-L. Chen, S. Chyntara, J.P. Chu, M.-J. Chen, S.-H. Chang, Beneficial effects of thin film metallic glass coating in reducing adhesion of platelet and cancer cells: Clinical testing, Surf. Coatings Technol. 344 (2018) 312–321, https://doi.org/10.1016/j.surfcoat.2018.03.040.

[87] M.A. Alfarsi, S.M. Hamlet, S. Ivanovski, Titanium surface hydrophilicity enhances platelet activation, Dent. Mater. J. 33 (6) (2014) 749–756, https://doi.org/10.4012/dmj.2013-221.
[88] Y. Jiang, Y. Li, C. Richard, D. Scherman, Y. Liu, Hemocompatibility investigation and improvement of near-infrared persistent luminescent nanoparticle ZnGa 2 O 4: Cr 3+ by surface PEGylation, J. Mater. Chem. B. 7 (2019) 3796–3803, https://doi.org/10.1039/C9TB00378A.
[89] T. Mattfeldt, G. Mall, Dipyridamole-induced capillary endothelial cell proliferation in the rat heart–a morphometric investigation, Cardiovasc. Res. 17 (4) (1983) 229–237, https://doi.org/10.1093/cvr/17.4.229.
[90] J.M. Bekisz, R.L. Flores, L. Witek, C.D. Lopez, C.M. Runyan, A. Torroni, B.N. Cronstein, P.G. Coelho, Dipyridamole enhances osteogenesis of three-dimensionally printed bioactive ceramic scaffolds in calvarial defects, J. Cranio-Maxillofac. Surg. 46 (2) (2018) 237–244, https://doi.org/10.1016/j.jcms.2017.11.011.
[91] P.F. Sánchez, E.M. Brey, J.C. Briceño, Endothelialization mechanisms in vascular grafts, J. Tissue Eng. Regen. Med. 12 (11) (2018) 2164–2178, https://doi.org/10.1002/term.2747.
[92] M. Bode, M. Mueller, H. Zernetsch, B. Glasmacher, Electrospun vascular grafts with anti-kinking properties, Curr. Dir. Biomed. Eng. 1 (2015) 524–528, https://doi.org/10.1515/cdbme-2015-0125.
[93] D.J. Wu, K. van Dongen, W. Szymczyk, P.J. Besseling, R.M. Cardinaels, G. Marchioli, M.H.P. van Genderen, C.V.C. Bouten, A.I.P.M. Smits, P.Y.W. Dankers, Optimization of anti-kinking designs for vascular grafts based on supramolecular materials, Front. Mater. 7 (2020), https://doi.org/10.3389/fmats.2020.00220.
[94] P. Robles-Martinez, X. Xu, S.J. Trenfield, A. Awad, A. Goyanes, R. Telford, A.W. Basit, S. Gaisford, 3D printing of a multi-layered polypill containing six drugs using a novel stereolithographic method, Pharmaceutics 11 (2019) 274, https://doi.org/10.3390/pharmaceutics11060274.
[95] Z.-L. Farmer, J. Domínguez-Robles, C. Mancinelli, E. Larrañeta, D.A. Lamprou, Urogynecological surgical mesh implants: new trends in materials, manufacturing and therapeutic approaches, Int. J. Pharm. 585 (2020) 119512, https://doi.org/10.1016/j.ijpharm.2020.119512.
[96] E. Mathew, J. Domínguez-Robles, E. Larrañeta, D.A. Lamprou, Fused deposition modelling as a potential tool for antimicrobial dialysis catheters manufacturing: new trends vs conventional approaches, Coatings 9 (2019) 515, https://doi.org/10.3390/coatings9080515.